~~Groundwater in terrestrial systems modelling: a new climatology~~ Impact of ~~extreme~~ 3D groundwater dynamics on heat events in historical regional climate simulations over Europe

Liubov Poshyvailo-Strube[1,2], Niklas Wagner[1,2], Klaus Goergen[1,2], Carina Furusho-Percot[3], Carl Hartick[1,2,4], and Stefan Kollet[1,2]

[1]Institute of Bio- and Geosciences: Agrosphere (IBG-3), Forschungszentrum Jülich GmbH, Jülich, Germany
[2]Centre for High-Performance Scientific Computing in Terrestrial Systems (HPSC TerrSys), Geoverbund ABC/J, Jülich, Germany
[3]National Research Institute for Agriculture, Food and Environment (INRAE), Avignon, France
[4]Jülich Supercomputing Centre (JSC), Forschungszentrum Jülich GmbH, Jülich, Germany

Correspondence: Liubov Poshyvailo-Strube (l.poshyvailo@fz-juelich.de)

Abstract. ~~Due to climate change, years with positive temperature anomalies are becoming more frequent in Europe, requiring high-resolution climate data to plan for climate change mitigation and adaptation. However, many~~ The representation of groundwater processes is simplified in most regional climate models (RCMs)~~simplify the representation of groundwater processes,~~ , potentially leading to biases in simulated ~~extreme heat events.~~ heat waves. Here, we ~~study the characteristics of summer heat events in~~ introduce a unique dataset from the regional Terrestrial Systems ~~Modeling~~ Modelling Platform (TSMP) ~~simulations, compared to an ensemble of EURO-CORDEX~~ forced by Max Planck Institute Earth System Model at Low Resolution (MPI-ESM-LR) boundary conditions for a historical time span in the context of dynamical downscaling of global climate models (GCMs) for climate change studies. TSMP explicitly represents 3D subsurface and groundwater hydrodynamics together with overland flow, closing the water and energy cycle from the bedrock to the top of the atmosphere. We perform an analysis of summer heat events (i.e. a series of consecutive days with a near-surface temperature exceeding the 90th percentile) for the historical time period 1976-2005 relative to the reference period 1961-1990 in a TSMP climate change scenario control ~~simulations, for the historical time period 1976-2005.~~ run. For comparison, the analysis is repeated for an ensemble of GCM-RCM simulations with simplified groundwater dynamics from the Coordinated Regional Climate Downscaling Experiment initiative for the European domain (EURO-CORDEX).

~~Our~~ While our results show that ~~in TSMP , the impact of groundwater coupling on the frequency of hot summer days depends on the considered time period and the region, associated with respective evaporative regime. An increasing trend of the frequency of hot summer days averaged across Europe is the lowest in TSMP compared to the other RCMs considered. Groundwater coupling has a systematic effect on the duration and intensity of heat events: summer heat events with long duration and high intensity are less frequent in TSMP compared to~~ TSMP simulates heat events consistently with the CORDEX ensemble, there are some systematic differences that we attribute to the representation of groundwater in TSMP. Compared to the CORDEX ensemble, TSMP simulates lower means and lower interannual variability in the number of hot days (i.e., days with a near-surface temperature exceeding the 90th percentile) on average over Europe. The decadal change in the number of

hot days is also lower in TSMP than on average in the CORDEX ensemble. ~~In particular, extended heat events with a duration exceeding 6 days,~~ TSMP systematically simulates fewer heat waves (i.e.~~heat waves, occur on average in Europe about 1.5-8 times less often in TSMP, while single-day heat events happen slightly moreoften in TSMP~~ , heat events lasting 6 days or more) compared to the CORDEX ensemble~~. The frequency of high-intensity heat waves in TSMP is up to 12 times lower on average in Europe compared to the CORDEX ensemble. Thus~~, moreover, they are less intense. Southern Europe is particularly sensitive to groundwater coupling, while Scandinavia is the least sensitive. Therefore, an explicit ~~groundwater representation~~ representation of groundwater in RCMs may ~~lead to rarer and weaker heat wavesin Europe also in climate projections. The findings of this work indicate an existing discrepancy in the ensemble of EURO-CORDEX climate change scenario control simulations and emphasize~~ be a key in bias reduction in simulated duration and intensity of heat waves, especially in Southern Europe. The results emphasise the importance of groundwater ~~representation in RCMs.~~ coupling in long-term regional climate simulations and potential implications for climate change projections.

1 Introduction

~~The number of extreme heat events has increased in recent decades (e.g., Frich et al., 2002; Alexander et al., 2006; Christidis et al., 2015; Z~~ ~~. Especially,~~ Over the past decades, the number of heat waves has increased (e.g., Frich et al., 2002; Alexander et al., 2006; Christidis et al., . The years 2003, 2010, ~~and~~ 2018, and 2022 were exceptionally hot ~~years~~ in Europe, characterised by record-breaking air temperatures ~~(e.g., Stott et al., 2004; Barriopedro et al., 2011; Liu et al., 2020; Dirmeyer et al., 2021)~~(e.g., Stott et al., 2004; Barriopedro et al. . With projected climate change, the ~~frequency of such extreme events will~~ occurrence of heat waves will continue to increase (e.g., Russo et al., 2015; Myhre et al., 2019; Hari et al., 2020; Molina et al., 2020; Masson-Delmotte et al., 2021), leading to multiple negative socio-economic impacts ~~(e.g., Bosello et al., 2007; Ciscar et al., 2011; Amengual et al., 2014; Naumann et al., 2021)~~ ~~.~~(e.g., Bosello et al., 2007; Ciscar et al., 2011; Amengual et al., 2014; Yin et al., 2022).

The underlying hydrometeorological mechanisms of heat ~~events~~ waves have been extensively studied ~~(e.g., Lhotka and Kyselý, 2015; Ho~~ ~~. The evolution of extreme heat events or heat waves depends primarily on the synoptic weather patterns in combination with ambient soil moisture conditions, further altered by multiple land-atmosphere feedback processes (e.g., Fischer et al., 2007; Horton et al., 2~~ ~~.~~ (e.g., Lhotka and Kyselý, 2015; Horton et al., 2016; Liu et al., 2020). Heat waves are triggered by strong, persistent quasi-stationary large-scale high pressure systems ~~with subsiding,~~ associated with atmospheric blocking events, resulting in subsiding, adiabatically warming air masses~~and atmospheric blocking events, as well as clear skies that enable a high amount of solar radiation (Tomczyk and Bednorz, 2016; Horton et al., 2016). Moreover, atmospheric blocking events impact winter/~~, and clear skies allowing for high insolation (Tomczyk and Bednorz, 2016; Horton et al., 2016; Kautz et al., 2022). Atmospheric blocking events also impact winter and early spring precipitation ~~over most of Europe, affecting soil moisture (e.g., Vautard et al., 2007; Ionita et al.,~~ ~~.~~ in most parts of Europe and, in turn, affect soil moisture (e.g., Vautard et al., 2007; Ionita et al., 2020). The evolution of heat waves depends primarily on the synoptic weather patterns in combination with ambient soil moisture conditions, further altered by multiple land-atmosphere feedback processes (e.g., Fischer et al., 2007; Horton et al., 2016).

Many European summer heat waves were preceded by a deficiency of spring precipitation (Dirmeyer et al., 2021; Stegehuis et al., 2021; Hartick et al., 2021). ~~The effect of~~ Due to the soil moisture memory ~~, associated with long-term (from weeks to months) persistence of wet or dry anomalies, allows to preserve the hydroclimatic conditions of preceding months (Martínez-de la Torre and Miguez-Macho, 2019; Song et al., 2019). Thus~~effect, the lack of precipitation in early spring causes negative soil moisture anomalies in early summer ~~,~~ and leads to ~~a stronger moisture-limited~~ strong land-atmosphere coupling (a measure of the response of the atmosphere to anomalies in the land surface state) with a lower evaporation fraction. ~~As a result, latent cooling decreases~~ This reduces latent cooling and amplifies summer temperatures ~~(e.g., Fischer et al., 2007; Miralles et al., 2012; Erd~~ ~~. Apart from precipitation, soil moisture content and distribution are strongly affected by subsurface hydrodynamics through vertical and lateral fluxes that connect groundwater with the land surface. In this connection~~(e.g., Fischer et al., 2007; Miralles et al., 2012; ~~l~~ . Note that soil moisture memory is a phenomenon of persistence of wet or dry anomalies over a long period of time, from weeks to months, after the atmospheric conditions that caused them have passed; this allows to preserve the hydroclimatic conditions of the preceding months (e.g., Manabe and Delworth, 1990; Song et al., 2019). Thus, depending on soil moisture conditions, the soil moisture memory effect can contribute to either buffering negative droughts impacts and weakening a heat wave, or, conversely, delaying drought recovery and exacerbating the occurrence of a heat wave (e.g., Erdenebat and Tomonori, 2018; Martínez-de la ~~l~~ . In addition to precipitation, soil moisture is strongly influenced by groundwater dynamics via vertical fluxes across the water table (capillary rise) and via horizontal fluxes through gravity-driven lateral transport within the saturated zone. Here, the water table depth ~~influences~~ dictates the intensity of shallow groundwater–soil moisture and ~~soil moisture-temperature coupling (Barlage et al., 2015; Keune et al., 2016; Mu et al., 2021).~~ evapotranspiration coupling (Kollet and Maxwell, 2008).

In the context of ~~e.g. climate change impact studies~~climate impact assessments, dynamical downscaling of ~~global climate models (GCMs) with regional climate models (RCMs) provides the required high-resolution climate information (Taylor et al., 2012; Mear~~ ~~. Most of the multi-model RCM ensemble simulations performed over Europe follow the common protocol of the Coordinated Regional Climate Downscaling Experiment for European domain (EURO-CORDEX) (e.g., Gutowski et al., 2016; Jacob et al., 2020) , which originated from two former European regional climate modelling projects, PRUDENCE (Christensen and Christensen, 2007) and ENSEMBLES (van der Linden and Mitchell, 2009).~~

~~Although~~ GCMs with RCMS is widely used to generate regional climate change scenario information (Vautard et al., 2013b; Mearns et al ~~.~~ RCMs have been shown to provide added value to ~~the driving GCMs (Giorgi and Gutowski, 2015; Prein et al., 2016; Rummukainen, 2016 , they may also lead to more noisy simulation results (e.g., Sørland et al., 2018). Despite the improved land-atmosphere coupling in RCMs, the representation of subsurface processes, i.e. groundwater dynamics and its coupling with the land surface and atmosphere, is generally~~ driving GCMs by better capturing small-scale processes (Giorgi and Gutowski, 2015; Torma et al., 2015; Prein et a , but model biases (offset during the historical period against observations) and uncertainties in climate projections still remain (Hawkins and Sutton, 2009; Lhotka et al., 2018; Sørland et al., 2018; Fernandez-Granja et al., 2021). In fact, many RCMs tend to overestimate the frequency, duration, and intensity of heat waves (Vautard et al., 2013a; Plavcová and Kyselý, 2016; Lhotka et al., 2018; ~~.~~

The role of soil moisture in modelling heat waves is crucial (e.g., Seneviratne et al., 2006, 2010; Fischer et al., 2007), but due to the complexity of the feedbacks involved and related high computational cost, the explicit representation of hydrological

processes is oversimplified or neglected in ~~existing~~ most RCMs. Commonly applied hydrology schemes ~~in RCMs are typically~~ are based on 1D-parameterizations in the vertical direction with ~~gravitational~~ runoff generation at the land surface and a gravity driven free drainage approach as the ~~boundary condition at the bottom, and runoff generation at the land surface. Thus, while in RCMs there is generally~~ lower boundary condition; in such a parametrisation there is no lateral subsurface flow ~~in such a 1D-column parametrisation and often~~ and only the 1D-Richards' equation is solved ~~(Niu et al., 2007; Campoy et al., 2013), some improvements have been made with respect to more operational groundwater parameterizations (Schlemmer et al., 2018) . Barlage et al. (2015), Keune et al. (2016)~~ (e.g., Niu et al., 2007; Campoy et al., 2013). RCMs with a simplified representation of hydrological processes have difficulties in reliably reproducing the land surface energy flux partitioning and, consequently, near-surface air temperatures, leading to warm biases (Vautard et al., 2013a; Barlage et al., 2021; Furusho-Percot et al., 2022). Hydrological parameters tuning (e.g., Teuling et al., 2009; Bellprat et al., 2016) or developing new parameterizations of groundwater dynamics (e.g., Liang et al., 2003; Yeh and Eltahir, 2005; Schlemmer et al., 2018) have been shown to improve model results. A physically consistent description of hydrological processes in RCMs can be achieved by an explicit representation of 3D subsurface and groundwater hydrodynamics together with overland flow. Thereby accounting for the feedback loops over the terrestrial system (e.g., Maxwell et al., 2007), i.e., the closure of water and energy cycles from groundwater across the land surface to the top of the atmosphere, as for instance in the Terrestrial Systems Modelling Platform (TSMP) (Shrestha et al., 2014; Gasper et al., 2014; Keune et al., 2016; Shrestha et al., 2018; Wunsch et al., 2022), a regional climate system model.

Keune et al. (2016) demonstrated the link between groundwater and near-surface air temperature in an analysis of the August 2003 European heat wave from TSMP simulations nested within ERA-Interim reanalysis (Dee et al., 2011). The model set up is over the CORDEX European domain (Gutowski et al., 2016; Jacob et al., 2020) with two different groundwater configurations: (i) simplified 1D free drainage approach and (ii) 3D physics-based variably saturated groundwater dynamics. The study clearly showed the impact of groundwater dynamics on the land surface water and energy balance: latent heat fluxes were higher and maximum temperatures were lower, especially in areas with shallow water table depth, in the 3D configuration compared to the simplified 1D free drainage approach. Keune et al. (2016) suggest that the 3D groundwater dynamics in TSMP alleviate the evolution of a single heat wave due to weaker land-atmosphere feedbacks compared to the simplified 1D free drainage approach, at least during the investigated European heat wave of summer 2003.

Therefore, compared to the 1D approach, the 3D groundwater dynamics in TSMP lead to regionally shallow groundwater levels, causing wetter soils, and a reduction in the Bowen ratio (i.e., ratio between sensible heat flux to latent heat flux) due to an increase in surface latent heat flux and ~~Furusho-Percot et al. (2022) showed that the energy flux partitioning and~~ a decrease in surface sensible heat flux, that leads to increased evapotranspiration (Maxwell and Condon, 2016). Such an increase in a latent heat flux also causes moistening of the lower atmosphere and increases downward longwave radiation due to the greenhouse effect of water vapor, on the other hand, it cools the surface and reduces outgoing surface longwave radiation (Pal and Eltahir, 2001). In addition, increased evapotranspiration may cause moist convection or rainfall, which further affects soil moisture (Eltahir, 1998; Yang et al., 2018). In its turn, the simplified representation of groundwater dynamics with the 1D free drainage approach leads to the opposite effect, namely an overestimation of the land surface-atmosphere coupling, i.e., ~~hence, near surface air temperatures are strongly influenced by groundwater, which also affects the representation of extreme~~

heat events.In fact, many RCMs overestimate the frequency, duration, andintensity of heat waves (e.g., Vautard et al., 2013a; Lhotka et al., 2 . deeper groundwater levels cause drier soils, an increase in the Bowen ratio, a decrease in cloud cover and enhancement of net solar radiation and a reduction in downward longwave radiation (Hartick et al., 2022), and, as a result, higher near-surface temperatures, which in turn further reduces soil moisture (Vogel et al., 2018). The ability of groundwater to decrease warm summer biases and moderate maximum air temperatures during a single seasonal heat wave in RCM simulations was also discussed in Barlage et al. (2015, 2021) and Mu et al. (2022).

To study the evolution of future heat events in Europe, here we first investigate the evolution of past heat events over the European continent in a multi-model RCM ensemble driven by CMIP5 (Taylor et al., 2012) GCM control simulations . The RCM ensemble is complemented with a new dataset from the regional Terrestrial Systems Modelling Platform (TSMP), which allows for an integrated groundwater-to-atmosphere simulations, thus closing the terrestrial water cycle from bottom to top. Further studies were carried out to understand whether the observed differences in simulated near-surface temperature due to differences in groundwater configuration persist over a long time period, and how this manifests itself for heat waves in the EURO-CORDEX realm. Furusho-Percot et al. (2019) showed that TSMP evaluation run (1996–2018) forced by the ERA-Interim reanalysis is able to capture climate system dynamics and the succession of warm and cold seasons on the regional scale for the PRUDENCE regions of Europe (Christensen and Christensen, 2007) consistently with E-OBS observations (Cornes et al., 201 . Furusho-Percot et al. (2022) demonstrated that TSMP multiannual simulations exhibit lower deviations of summer heat wave indices from the E-OBS observational dataset, compared to ERA-Interim driven RCM evaluation simulations of the EURO-CORDEX experiment, which tend to simulate too persistent heat waves. This particular behaviour of TSMP is attributed to its improved hydrology. The improved capacity to sustain soil moisture translates into more reliable latent heat flux and evapotranspiration, that, in turn, leads to a decrease in the heat wave intensity, spatial extent, and the number of days with anomalously high near-surface temperatures. An important question still remains: how will these findings be reflected in long-term regional climate simulations?

In this paper, we present a unique dataset from TSMP forced by the Max Planck Institute Earth System Model at Low Resolution, MPI-ESM-LR (Giorgetta et al., 2013), historical boundary conditions in the context of EURO-CORDEX GCM-RCM downscaling and long-term climate modelling. We interrogate the statistics of the heat event heat events (i.e., a series of consecutive days with a near-surface temperature exceeding the 90th percentile) characteristics (frequency, duration, intensity) for the summers of 1976-2005 with respect to the reference period 1961-1990 by comparing TSMP results with the EURO-CORDEX multi-model RCM ensemble driven by GCM control simulations of phase five of the Coupled Model Intercomparison Project (CMIP5) (Taylor et al., 2012), to understand the impact of groundwater dynamics influence of 3D groundwater dynamics on simulated heat events for historical regional climate simulations and potential consequences for ensuing climate change projections. While the 1996-2018 TSMP evaluation runs nested within ERA-Interim reanalysis were examined for heat wave statistics (Furusho-Percot et al., 2022), long-term historical climate simulations of TSMP forced by GCM have not been previously presented. Thus, this is the first downscaled regional historical climate simulation from groundwater across the land surface to the top of the atmosphere placed in the context of the climate scenario runs of the EURO-CORDEX RCM ensemble and analysed for summer heat events.

Section

In Sec. 2introduces TSMP and its setup , describes , we describe TSMP setup and configuration, the ensemble of the EURO-CORDEX climate change scenario RCM GCM-RCM control runs, and the heat event analysesmethodology of heat events analysis. In Sect. 3, we estimate examine the new GCM-RCM TSMP-MPI dataset for consistency with the CORDEX ensemble, and we present the results on the impact of groundwater 3D groundwater dynamics on simulated heat events frequency, duration, and intensity, and assess TSMP's characteristics in simulating European heat events compared to the CORDEX ensemble. for regional historical climate simulations. Section 4 provides a summary and overall conclusions.

2 Methods

2.1 The Terrestrial Systems Modelling Platform (TSMP)

TSMP is a scale-consistent, highly modular, fully integrated soil-vegetation-atmosphere modelling system (e.g., Shrestha et al., 2014; Gasper et al., 2014). In the applied climate mode setup, TSMP consists of three component models: the atmospheric model COSMO (COnsortium for Small Scale Modelling) (COSMO) model version 5.01 (Baldauf et al., 2011), the land surface model CLM ((e.g., Baldauf et al., 2011), the Community Land Model (CLM) version 3.5 (Oleson et al., 2004, 2008) (e.g., Oleson et al., 2004, 2008), and the hydrological model ParFlow version 3.2 (Kollet and Maxwell, 2006; Maxwell, 2013) (e.g., Maxwell and Miller, 2005; Kollet and Maxwell, 2006; Kuffour et al., 2020). The component models are externally coupled via the Ocean Atmosphere Sea Ice Soil (OASIS,) version 3.0) Model Coupling Toolkit (MCT) coupler (Valcke, 2013), which passes states and fluxes between individual TSMP component models (for details see Shrestha et al., 2014; Gasper et al., 2014) . In contrast to most RCMs, the TSMP closes (e.g., Valcke, 2013), which enables closure of the terrestrial water and energy cycles from the bedrock to the top of the atmosphere. For details on TSMP, see Shrestha et al. (2014); Gasper et al. (2014).

COSMO is a non-hydrostatic limited-area atmospheric model(e.g., Baldauf et al., 2011). The COSMO model It is based on the primitive thermo-hydrodynamical Euler equations formulated in rotated geographical coordinates and generalized terrain-following height coordinates, describing compressible flow in a moist atmosphere. COSMO parameterization schemes are responsible for cover various physical processes, such as radiation, cloud microphysics, deep convection, etc. The lateral boundary conditions used for COSMO are usually typically provided by a coarse grid model, for instance, GCMs or reanalyses. In . In the coupled setup of TSMP, the lower boundary conditions for COSMO (e.g., surface albedo, energy fluxes, surface temperature, surface humidity) are provided by the CLMland surface model via the component models couplingCLM.

CLM is a biogeophysical model of the land surface(e.g., Oleson et al., 2004, 2008). It simulates land-atmosphere exchanges in response to atmospheric forcings. CLM consist of four components that describe biogeophysics, hydrologic cycle, biogeochemistry, and dynamic vegetation. In TSMP, CLM receives short-wave radiation, wind speeds, barometric pressure, precipitation, near-surface temperature, and specific humidity from COSMO. In turn, CLM sends to ParFlow infiltration and evapotranspiration fluxes for each soil layer.

ParFlow is a hydrological model that simulates variably saturated three-dimensional subsurface hydrodynamics using Richards equation integrated with shallow overland flow based on a kinematic wave approximation(Ashby and Falgout, 1996; Maxwell and Miller, 2

. ParFlow allows 3D-redistribution of subsurface water in a continuum approach. In TSMP, ParFlow replaces the hydrologic functionality of CLM.

2.2 TSMP Model setupTSMP simulations were performed over Europe

TSMP simulations in this study are conducted for the historical time period from December 1949 to the end of 2005 over the European continent according to the EURO-CORDEX simulation protocol (e.g., Gutowski et al., 2016) . The TSMP simulations were set up on the using rotated latitude-longitude model grid with a horizontal resolution of 0.11° CORDEX grid, i.e approximately (EUR-11) or about 12.5 km. COSMO had a vertical range up Note, the simulations represent the first EURO-CORDEX climate change control simulations with explicit representation of 3D groundwater. COSMO extends vertically to 22 km , CLM had subdivided into 50 levels. The COSMO configuration used in the TSMP setup resembles that of the COSMO model in CLimate Mode (CCLM) (e.g., Rockel et al., 2008). CLM has 10 soil layers with a total depth of 3 m, while ParFlow reached a total depth of 57 m. COSMO contained 50 vertical levels, CLM had . These layers coincide with the 10 soil layers that coincided with the upper ParFlow layers . ParFlowhad a total of 15 layers with variable grid spacing increasing from top to bottomtop layers of ParFlow, which has 5 additional layers that increase in thickness to a total depth of 57 m. The time step of for ParFlow and CLM was is 900 secand , for COSMO it is 75 secfor COSMO. The coupling time step between the TSMP component models was is 900 sec.

The TSMP climate change scenario control simulations were conducted for the historical time period from December 1949 to the end of 2005 constituting the first climate control simulation with a groundwater to top-of-atmosphere terrestrial model. Land surface, subsurface hydrology, and energy states were initialized with the moisture conditions of 1st of December 2011 from a spun-up evaluation run driven by ERA-Interim reanalysis (Furusho-Percot et al., 2019), which influenced the first years of the simulations and discarded in the analyses due to hydrodynamic spin-up. Forcing data and the lateral boundary conditions for the TSMP atmospheric component model were provided by the Max-Plank Institute's MPI-ESM-LR r1i1p1 GCM experiment, with a resolution of T63L47 (Giorgetta et al., 2013).

Detailed information on CLM and ParFLow specifications used in the TSMP setup has already been described earlier in Furusho-Percot et al. (2019); Hartick et al. (2021). In addition to these studies , we For CLM, plant functional types (PFT) are taken from the Moderate Resolution Imaging Spectroradiometer (MODIS) dataset (Friedl et al., 2002). Leaf area index, stem area index, and the monthly bottom and top heights of each PFT are calculated based on the global CLM surface dataset (Oleson et al., 2008). Compared to the previous studies of Furusho-Percot et al. (2019, 2022); Hartick et al. (2021), where soil parameters were assumed to be vertically homogenous in ParFlow, in this work we have improved the subsurface geology using geological information from different databases as follows. We defined the soil texture hydrogeology, which is described below. Static input fields (i.e., soil color, percentage clay, percentage sand, dominant land use type, dominant soil types in the top 10 layersof ParFlow from the layers, dominant soil types in the bottom layers and subsurface aquifer and bedrock bottom layers) are derived from MODIS, Food and Agriculture Organization soil database (FAO, 1988). For the 5 lowest soil layers, we prescribed hydrogeology from the , pan-European River and Catchment Database (Vogt et al., 2007), International Hydrogeological map of Europe (IHME) dataset (Duscher et al., 2015) and (Duscher et al., 2015) and the GLobal HYdroge-

ology MaPS (GLHYMPS) ~~(Gleeson et al., 2014; Gleeson, 2018). As a proxy for alluvial aquifer systems in ParFlow, we used a~~ (Gleeson et al., 2014). In particular, the bedrock geology is constructed using the IHME dataset and the lower resolution GLHYMPS. The pan-European River and Catchment Database ~~(Vogt et al., 2007)~~ serves in ParFlow as a proxy for the alluvial aquifer system, with the assumption that alluvial aquifers lie underneath or in ~~close~~ proximity of existing rivers.

~~The TSMP output constitutes a dataset of all terrestrial essential climate variables at a 3-hourly time step.~~Forcing data for the TSMP atmospheric component model, i.e., for COSMO, are provided by the Max-Planck Institute's MPI-ESM-LR r1i1p1 CMIP5 GCM experiment, with a resolution of T63L47 (Giorgetta et al., 2013). CLM and ParFlow are initialised (i.e., land surface, subsurface hydrology, and energy states) with the moisture conditions of the 1st of December 2011 from the previous evaluation run driven by ERA-Interim reanalysis (Furusho-Percot et al., 2019). In the analysis, we discard the first 10 years of TSMP simulations due to hydrodynamic spin-up.

2.3 ~~The ensemble of~~ EURO-CORDEX ~~climate change scenario RCM control runs~~ensemble

~~The~~

The selected EURO-CORDEX ensemble members of the multi-physics RCM climate change scenario control runs driven by different CMIP5 GCMs (r1i1p1 ensemble members) on 0.11° grid (EUR-11) ~~grid~~ is used in conjunction with the coupled TSMP modelling platform to study the characteristics of summer heat events. ~~All RCM ensemble members, with the exception of~~ Note that CMIP5 GCM historical control simulations are performed under observed natural and anthropogenic forcing (Taylor et al., 2012). Based on availability, the following EURO-CORDEX simulations are considered, identified by their institution, and the RCM and GCM IDs (Table 1): CCLM4-8-17 (CCLM4-8-17 forced by MPI-ESM-LR and CNRM-CM5), CLMcom-ETH (COSMO-crCLIM forced by MPI-ESM-LR, CNRM-CM5, and NCC-NorESM1-M), MPI-CSC (REMO2009 driven by MPI-ESM-LR), GERICS (REMO2015 forced by NCC-NorESM1-M, NOAA-GFDL-ESM2G, and IPSL-CM5A-LR). The considered CORDEX multi-model ensemble includes two main groups of RCMs, namely COSMO (v5.01 in TSMP, v4.8, and an accelerated version of COSMO in COSMO-crCLIM) and REMO (v2009 and v2015), driven by 5 different GCMs, for a total of 10 different GCM-RCM pairs. For a reliable analysis, Giorgi and Coppola (2010) points out that a subset of at least 4-6 models is needed, and Déqué et al. (2007) shows that the number of GCMs involved should at least be the same as the number of RCMs. The CORDEX RCM most compatible with TSMP is CCLM4-8-17, where the largest differences arise from the lower boundary condition in COSMO. In TSMP, the lower boundary condition for COSMO accounts for groundwater feedbacks due to the coupling between the land surface model CLM and the hydrologic model ParFlow, unlike in the CCLM where the soil processes are modelled with the TERRA-ML soil-vegetation land surface model (Grasselt et al., 2008; Doms et al., 2013). All members of the ensemble, except for TSMP, include ~~only a highly~~ simplified representations of subsurface hydrodynamics. ~~An overview of the RCM ensemble with 10 model products is provided in Table 1.~~

Note that the ensemble of EURO-CORDEX climate change scenario RCM control runs is not intended for direct comparison between individual models, as it includes different RCMs in combination with different driving GCMs. Therefore, due to connections of various factors (e.g., model setups, conceptual and structural model uncertainties, different physical parameterizations, internal variability, representation of subsurface-land-atmosphere interactions, lower and lateral atmospheric GCM boundary

Table 1. ~~Details on~~ The ensemble of EURO-CORDEX ~~RCM~~ climate change scenario control runs~~used in the analysis~~.

~~Institution~~ GCM-RCM	~~RCM~~ MPI-ESM-LR ~~MPI-ESM-LR~~ *(Mauritsen et al., 2019)*	~~GCM forcing data~~ ~~FZJ~~ CNRM-CM5 *(Voldoire et al., 2013)*	~~TSMP *(Shrestha et al., 2014)*~~ NCC-NORESM1-M *(Bentsen et al., 2013)*
TSMP *(Shrestha et al., 2014)*	X	~~MPI-ESM-LR~~	
CCLM4-8-17 *(Rockel et al., 2008)*	X	~~MPI-ESM-LR~~ X	
~~MPI-CSC~~ COSMO-crCLIM *(Pothapakula et al., 2020)*	X	X	X ~~REMO2009 *(Jacob and Podzun, 1997)*~~
REMO2009 *(Jacob and Podzun, 1997)*	X	~~NCC-NorESM1-M~~	
REMO2015		~~IPSL-CM5A-LR *(Dufresne et al., 2013)*~~	X

conditions, etc.) in addition to the groundwater coupling, it is challenging in the multi-model CORDEX ensemble to reveal the exact cause and effect relationships of the explicit groundwater representation for simulated hot days and associated characteristics of heat events in RCMs. However, the consideration of an extended period, e.g., 30 years, allows to draw statistical conclusions. In this study, the aim of the analysis of the TSMP historic simulations in the context of the CORDEX RCM ensemble is to interrogate whether the new TSMP driven by MPI-ESM-LR GCM-RCM dataset is consistent with the CORDEX ensemble and, in particular, to gain insight into the role of groundwater for long-term climate simulations from the statistical analysis of heat events.

2.4 ~~Heat event analyses~~Analysis of heat events

There is no ~~generally accepted metric for~~ universally accepted method for defining heat events, ~~and in particular for heat waves. While there is an emphasis~~ but the most commonly used approach is built on a percentile temperature threshold (e.g., Zhang et al., 2005, 2011; Sulikowska and Wypych, 2020). Note that although the focus is on temperature-based diagnostics, ~~current methods are~~ it is often ambiguous or inconsistent, ~~with a focus on certain impacts or sectors,~~ describing heat events only partially (Perkins and Alexander, 2013). ~~The most commonly used approach is built on the percentile temperature threshold (e.g., Zhang et al., 2005, 2011).~~

In this study, we define ~~the start of a heat event as the first day with the mean daily~~ a hot day as a day with a daily mean temperature above the local 90th percentile ~~(e.g., Vautard et al., 2013a). The~~ from the reference 1961-1990 period. We calculate the 90th percentile ~~is calculated for each~~ for each EUR-11 grid point of the EURO-CORDEX domain for ~~each~~ every summer day from a consecutive 5-day moving window centered on ~~each calendar day of~~ that calendar day from the 30-year reference period ~~from~~ between 1961 ~~to~~ and 1990. ~~We assume that a day with the mean daily temperature exceeding the 90th percentile is a hot day (e.g., Sulikowska and Wypych, 2020)~~The first occurrence of a hot day determines the start of a heat event. A series of hot days constitutes a heat event, highlighted in dark red in Fig. 1. A ~~series of hot days constitute a heat event. A~~ heat event is interrupted if the mean daily temperature drops below the 90th ~~percentile. The cumulative~~ percentile-based threshold. The total number of hot days during ~~a heat event~~ the investigated period corresponds to the TG90p heat index

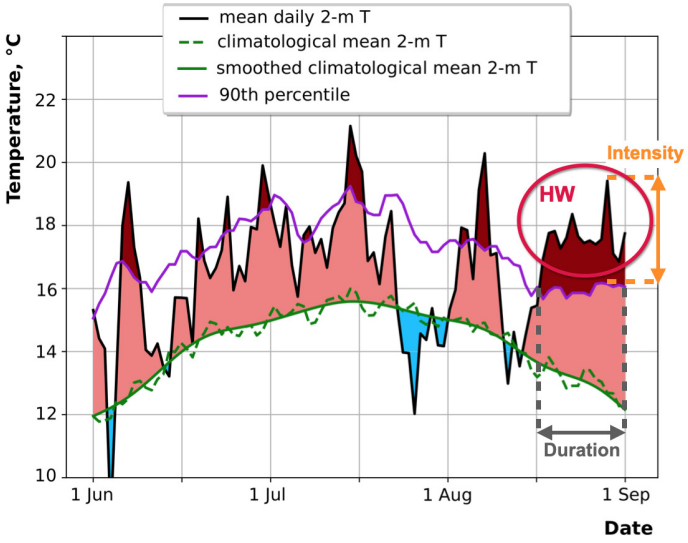

Heat event #	Start date	End date	Duration, days	Intensity, °C
1.	1.06	1.06	1	0,26
2.	6.06	9.06	4	2,71
3.	19.06	19.06	1	1,30
4.	24.06	24.06	1	1,07
5.	30.06	1.07	2	1,40
6.	7.07	7.08	2	0,41
7.	15.07	17.07	3	1,90
8.	3.08	4.08	2	0,63
9.	6.08	7.08	2	3,08
10.	17.08	31.08	15	3,28

Figure 1. Schematic of summer heat wave (HW) detection. An example is given for June-July-August of 1972 for one grid point [250, 300] of the EURO-CORDEX domain. Data taken from the TSMP simulations. The solid black line is the mean daily 2 m air temperature. The dashed green line represents the climatological (1961-1990) mean daily 2 m air temperature, and the solid green line represents the same dependence with a Butterworth filter. The solid violet line is the 90th percentile of the mean daily 2 m air temperature in summer calculated from a 5-day window centered on each calendar day for the 1961-1990 reference period. The shaded light red colour indicates days with temperatures above the climatological mean, and the shaded dark red colour emphasizes days with temperatures above the 90th percentile, i.e. "hot days", "heat events", or "heat waves".

~~, introduced by the European Climate Assessment and Dataset (ECA&D) project, complementing the core set of indices determined by the~~ from the joint CCl/CLIVAR/JCOMM Expert Team on Climate Change Detection and Indices (ETCCDI) ~~(e.g., Frich et al., 2002; Zhang et al., 2011).~~ (e.g., Karl et al., 1999). TG90p describes the number of days with

$TG_{ij} > TG_{in}90,$

$TG_{ij} > TG_{in}90,$ where TG_{ij} is the mean daily temperature on day i of period j ~~,~~and $TG_{in}90$ is the i-day 90th percentile ~~of mean daily temperature calculated for a 5-day window centred on each calendar day of the~~ calculated from a 30-year reference period n.

~~Schematic of the methodology to detect a heat wave (HW) during the summer season. An example is given for June-July-August of 1972 for one grid point 250, 300of the EURO-CORDEX domain. Data taken from the TSMP simulations. The solid black line is the mean daily 2-m air temperature in the summer of 1972. The dashed and solid green line represents the climatological raw average daily 2-m air temperature and Butterworth filtered data between 1961 to 1990, respectively. The solid violet line is the 90th percentile of the mean daily 2-m air temperature calculated from a 5-day window centered on each calendar day of~~

the 1961-1990 reference period. The shaded light red colour indicates days with temperatures above the climatological mean, and the shaded dark red colour emphasizes days with temperatures above the 90th percentile, which we define as "hot days".

A heat event can be characterised by its duration, intensity, and frequency (e.g., Horton et al., 2016). A heat event duration is the number of consecutive days over which the heat event lasts. If a heat event lasts long enough, it can be classified as a heat wave. Similar to Fischer and Schär (2010), we define consider a heat wave as a spell of at least six consecutive days with mean daily temperatures above the local 90th percentile of the reference period (1961-1990). For explanation, period. See Fig. 1 shows an example of a heat wave with the duration of 15 days. Note that the use of terms "heat event" and "heat wave"is similar in the context of this paper, with for an explanation of the heat wave detection. Therefore, we consistently use the terminology "hot day", "heat event"referring to a series of unusually hot days. Furthermore, low-intensity heat events are also mentioned in literature as either a single-day or a multi-day event over a temperature threshold between the 85 and 92.5th percentile (Strathearn et al., 2022). In addition, some authors classify heat waves as low-intensity, severe, and extreme (Nairn and Fawcett, 2014)., and "heat wave" throughout this analysis.

In our analysis, a

A heat event intensity , HEI_m, is the maximum of the difference between the mean daily temperature and the calendar day 90th percentile within an individual heat event m (e.g., Vautard et al., 2013a; Habeeb et al., 2015):

$$HEI_m = max(TG_{im} - TG_{in}90),$$

where TG_{im} is the mean daily temperature on day i during the heat event m. The intensity of the reference 1961-1990 period within a single heat event (e.g., Vautard et al., 2013a). Intensity represents the severity of a heat event , (see Fig. 1). Adopting the definition from the heat wave duration index (e.g., Frich et al., 2002; Espírito Santo et al., 2014), we classify a heat wave as intense if it exceeds 5 K. Some studies also classify heat waves according to their intensity as low, severe, or extreme (e.g., Nairn and Fawcett, 2014).

The 90th percentile of 2-m air temperatures averaged over the summer season simulated with TSM. The 90th percentile is obtained from a consecutive 5-day moving window centered on each calendar day of the summer season of the 30-year reference period from 1961 to 1990. The white border indicates the focus domain for the heat event analysis in our study 10°W-30°E, 36°N-70°N. The smaller boxes with the respective abbreviations are the PRUDENCE regions: British Isles (BI), Iberian Peninsula (IP), France (FR), Mid-Europe (ME), Scandinavia (SC), Alps (AL), Mediterranean (MD) and Eastern Europe (EA).

We define the frequency of heat events of a certain type, HEF_k, as the number of such heat events divided by the total number A frequency of heat events (e.g., Vautard et al., 2013a):

$$HEF_k = \sum_{l=1}^{L} HE_{kl} / \sum_{j=1}^{J} HE_j,$$

where HE indicates a heat event, k denotes a specific feature of a heat event of a certain type (e.g., heat events of a certain specific duration or intensity) , l is the ordinal counter of a heat event of a certain type k within the total number L of heat

events of this type, *j* is the ordinal counter of any heat event within during the investigated period is the number of specific heat events divided by the total number *J* of all heat events . For instance, from that occurred during this investigated period (e.g., Vautard et al., 2013a). For example, in Fig. 1, the frequency of heat events with the duration of 2days during the summer season is equal to days duration is the number of 2-day heat events (4 events) those heat events (i.e., 4) divided by the total number of all heat events (i.e., 10events). The resulting frequency is 0.4 and indicates that 40% of all heat events during the considered summer period have the have a duration of 2 days. Based on this definition, we estimate the frequency of hot days in summer as the number of hot days, or the TG90p index (33 days, see Fig. 1), divided by the total number of days in the summer season (92 days). The estimated frequency of hot days is approximately 0.36, indicating that 36% of all summer days are classified as hot days.

In this study, we examine past

We examine heat events in Europe during the summer season, evaluating their characteristics , such as frequency, duration, and intensity, based on the mean daily 2-m by assessing their characteristics explained above based on mean daily 2 m air temperatures on the native EURO-CORDEX EUR-11 grid in the ensemble of EURO-CORDEX climate change scenario RCM control runs driven by different GCMs, as listed in Table 1. The analysis is performed for the summer season of the 30-year period1976-2005, , from 1976 to 2005 with regard to the reference period from 1961 to 1990 in each RCM. The analysis is adopted from the work of Vautard et al. (2013a) and conducted over the arbitrarily chosen focus domain covering the European continent [10°W-30°E, 36°N-70°N] as shown in Fig. 2.

3 Results and Discussion

2.1 Influence of groundwater on the number of hot days in summer

Note that we analyse only land grid elements.

Cumulative number of hot days (TG90p index) during June-July-August. The example is shown for arbitrary selected years 1990, 1995, 2000, and 2005. The TG90p index is shown from the TSMP simulations (a, b, c, d) and CCLM simulations (e, f, g, h), their absolute differences are presented in (i,j, k, l).

We estimate the cumulative number

3 Results

3.1 Hot days number

In order to evaluate the impact of groundwater coupling on the interannual variability of hot days , during the summer season in RCMs, we examine the occurrence of hot days in the focus domain in the ensemble of the EURO-CORDEX climate change scenario GCM-RCM historical control runs from 1976 to 2005 with regard to the reference period 1961-1990. A comparison of the mean hot days number (i.e., TG90p index, for each summer season during 1976-2005. The results from two regional climate

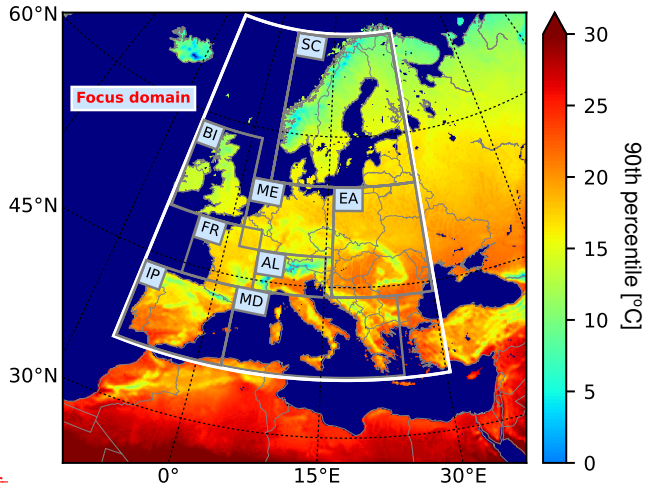

Cumulative number

Figure 2. Mean of hot days (TG90p index) during the summer season 90th percentile of 2003 for RCMs 2 m air temperatures in summer simulated with TSMP. The 90th percentile is calculated from a consecutive 5-day moving window centered on each calendar day of the ensemble of EURO-CORDEX climate change scenario control runs (see Table 1), with respect to summer season from the 30-year reference period 1961-1990. from 1961 to 1990. The absolute differences in white box indicates the TG90p index between TSMP and RCMs focus domain for the analysis in our study [10°W-30°E, 36°N-70°N]. PRUDENCE analysis regions are also shown . Green and yellow as grey boxesunderline examples of different groups of ensemble member: British Isles (BI), e.g.Iberian Peninsula (IP), different RCMs driven by the same GCMsFrance (FR), the same RCMs driven by different GCMsMid-Europe (ME), Scandinavia (SC), Alps (AL), Mediterranean (MD) and Eastern Europe (EA).

models, the Terrestrial Systems Modelling Platform (TSMP) and CCLM (COSMO model in CLimate Mode; e.g., Rockel et al., 2008; Steg , for several years are shown in index) per summer over the focus domain from TSMP and the CORDEX ensemble suggests that the impact of groundwater coupling varies from year to year (Fig. **??** as an example. Both RCMs, TSMP and CCLM, are driven by 3). Here, the same forcing data from the Max-Plank Institute's MPI-ESM-LR r1i1p1 GCM experiment (e.g., Giorgetta et al., 2013) . In addition, long-term soil moisture memory effects can play an important role, for example by increasing the probability of a water deficit in regions that had a water deficit in the previous year (e.g., Hartick et al., 2021), and consequently influencing the hot days occurrence. A positive linear trend in the TG90p index is observed in all considered RCMs on average in the focus domain (see Fig. 3). The decadal change in the TG90p index in TSMP is 1.53 days. In contrast, the TSMP atmospheric component model is CCLM compliant (see Sect. 2.1). The lower boundary condition for the TSMP atmospheric component model includes the groundwater feedback due to the coupling between the land surface component model CLM and the hydrologic component model ParFlow, unlike in the CCLM where the soil processes are modelled with the TERRA-ML soil-vegetation land surface model. (e.g., Grasselt et al., 2008; Doms et al., 2013; Schulz et al., 2016). decadal change in the TG90p index averaged over the multi-model RCM CORDEX ensemble (excluding TSMP) is higher, up to 2 days.

There is good agreement in the overall pattern

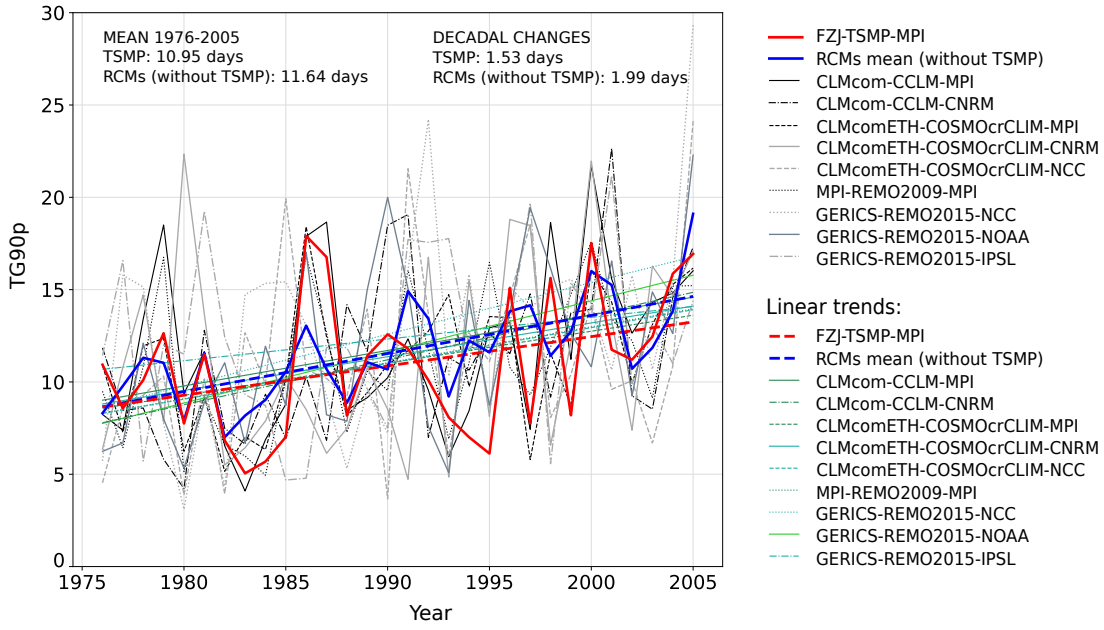

Figure 3. Time series of the mean hot days number (TG90p index) during the summer season over the focus domain and its linear trends during 1976-2005 with respect to the reference period 1961-1990, in the ensemble of EURO-CORDEX climate change scenario RCM control runs. Averaging of TG90p is performed over the total number of land grid points in the focus domain. The solid and dashed red lines show the TG90p mean from the TSMP simulations, as well as its linear trend. The black and grey lines represent the TG90p mean from the CORDEX ensemble and the different green lines are their linear trends respectively. The TG90p averaged over the multi-model RCM CORDEX ensemble (excluding TSMP) is shown with the solid blue line and its linear trend is shown with the dashed blue line.

A spatial distribution of the TG90p ~~index calculated from TSMP and CCLM output. In 1990, with the exception of Northern Europe, TSMP shows larger~~ mean and TG90p ~~values compared to CCLM (~~variability, as well as the decadal change of TG90p is shown in Fig. ~~??~~i). ~~This year, the largest difference in the~~ 4-6. Uncertainty in simulated near-surface temperature in summer is strongly controlled by the large-scale atmospheric circulation imposed by the boundary conditions (e.g., Déqué et al., 2007; Fernández et al., 2019), with larger impact in the South-West (IP, FR) than the North-East (SC, ME, EA) PRUDENCE regions (Déqué et al., 2012). Hence the spatial pattern of the TG90p index ~~between TSMP and CCLM is found in the Alps, reaching 15 days or more. Similar behaviouris observed also in 2005 with higher~~ significantly differs between different GCM-RCMs and the results from RCMs driven by the same GCMs show a rather similar behaviour. TSMP produces the smoothest spatial distribution of the TG90p ~~values in Central and Southern Europe in TSMP compared to CCLM (~~mean and TG90p variability compared to the CORDEX ensemble (see the standard deviation indicated in Fig. ~~??~~l). ~~Unlike in 1990 and 2005, TSMP simulated fewer hot summer days than CCLM in 1995 and 2000, with a significant difference of more than 15 days in Central and Southern Europe (Fig. ??j, k). Thus, the impact of groundwater coupling apparently varies from year to year and also depends on the region under consideration. The effects of soil moisture memory can play an important role here by buffering droughts and weakening heat events. In contrast, past drought condition may be memorized in groundwater~~

storage causing a delay in its recovery, and hence exacerbating the occurrence of heat events due to a reduction of latent heat and enhanced surface sensible heat flux (e.g., Erdenebat and Tomonori, 2018; Martínez-de la Torre and Miguez-Macho, 2019; Hartick et al., 20

.

The 4, 5). Thus, in TSMP, the regional difference in the distribution of the hot days number is smaller, and the climate is more steady with respect to the interannual changes in the simulated number of hot days in summer. In the considered ensemble, the TG90p index for the EURO-CORDEX ensemble (see Table 1) for 2003 as an example is shown in mean and TG90p variability averaged over the focus domain are lowest in TSMP driven by MPI-ESM-LR, 10.95 days and 6.80 days, respectively, and highest in REMO2015 driven by NCC-NorESM1-M, 12.72 days and 9.42 days, see Fig. **??**. The considered ensemble members can be classified into three groups with respect to the used RCMs and GCMs forcing data: different RCMs driven by the same GCMs, the same RCMs driven by different GCMs, and different RCMs driven by different GCMs.The overall pattern of A1-A2 in Appendix A for details. The decadal change in the TG90p index averaged over the focus domain ranges from the lowest value of 1.13 days in REMO2015 driven by IPSL-CM5A-LR and the highest of 2.68 days in REMO2015 driven by NOAA GCM (Fig. A3 in Appendix A).

In particular, the TG90p index calculated from different simulated by TMSP is consistent with the CORDEX RCMs driven by the same GCMs (MPI-ESM-LR GCM, although there are some regional differences (see Fig. **??**a-g, h-k, l-o)agrees relatively well for 2003, although discrepancies in the exact magnitude and the spatial extent of 4a-d, Fig. 5a-d). The largest differences are found in the Iberian Peninsula, where TSMP produces the TG90p are detectable. The differences of mean of 10.36 days and the TG90p from the same RCMs driven by different GCMs (e.g., mean simulated by the CORDEX MPI-ESM-LR driven RCMs is 12.54-12.75 days (see Fig. **??**d, h or Fig. **??**f, j, n)are comparable with the differences from different A1 in Appendix A). At the same time, the interannual TG90p variability in the Iberian Peninsula reaches 6.17 days in TSMP and 8.01-9.59 days in the CORDEX MPI-ESM-LR driven RCMs (see Fig. A2 in Appendix A). All considered RCMs driven by the same GCMs. But in some cases the same RCM driven by different GCMs MPI-ESM-LR simulate a negative decadal change in the TG90p index in Scandinavia, and a positive decadal change is observed in Southern and Central Europe (Fig. **??**l, p, s) has a significant difference 6a-d). TSMP simulates, on average, a lower decadal change in the TG90p index (e.g. in the focus domain than the CORDEX RCMs driven by MPI-ESM-LR (see Fig. A3 in Appendix A). The largest differences in the decadal change of the TG90p appear over the Iberian Peninsula, 30 days or even more in the Iberian Peninsula), emphasizing a strong influence of the lateral boundary conditions from the different GCMs.Note that REMO2015, driven by NOAA and IPSL, imposes different distributions of the where TSMP produces 2.26 and CORDEX RCMs driven by MPI-ESM-LR simulate an increase of 3.66-4.25 hot days per decade.

From a comparison of TSMP and its most compatible CORDEX RCM, i.e., CCLM driven by MPI-ESM-LR, with the largest differences in the lower boundary condition for COSMO accounting for groundwater feedbacks in TSMP, TSMP simulates overall lower TG90p index (e.g., high values in mean and TG90p variability in all PRUDENCE regions, with the largest discrepancies over the Iberian Peninsula) compared to the RCMs of the EURO-CORDEX ensemble, likely due to discrepancies in the large-scale atmospheric circulation in the driving GCMs. Furthermore, and the Mediterranean and the smallest differences in Scandinavia. The decadal change in the TG90p differences shown in Fig. **??** highlight the different is

also lower in all PRUDENCE regions except the Alps and Eastern Europe. Different responses to groundwater coupling in ~~the regions of~~ different PRUDENCE regions may be explained by the soil moisture-temperature feedback associated with different evaporative regimes, energy-limited ~~(Scandinavia and Northeastern Europe) and~~ in Scandinavia and Northern Europe versus moisture-limited ~~(Southern and Southeastern Europe) regimes.~~

~~Groundwater impact on the frequency of hot daysDue to connections of various factors other than groundwater coupling in the multi-model CORDEX ensemble (e.g., various model setups, conceptual and structural model uncertainties, different physical parameterizations, internal variability, representation of subsurface-land-atmosphere interactions, lower and lateral atmospheric GCM boundary conditions) , it is challenging to reveal the exact cause and effect relationship of the explicit groundwater representation for simulated hot days and the associated heat events characteristics in RCMs. Moreover, the ensemble of EURO-CORDEX climate change scenario RCM control runs is not intended for direct comparison between individual models, as it includes different RCMs in combination with different driving GCMs.However, as has been shown in previous studies, the consideration of an extended period, e.g., 30-years, allows to draw statistically conclusions.~~

~~Time series of the mean frequency of hot summer days in~~ in Southern Europe ~~(averaged over the focus domain) and its linear trends during 1976-2005 with respect to the reference period 1961-1990, in the ensemble of EURO-CORDEX climate change scenario RCM control runs (see Table 1). The solid and dashed red lines show the mean frequency of hot days in summer from the TSMP simulation, as well as its linear trend. The black and grey lines represent the RCM ensemble frequencies of hot days, the shaded blue area represents their standard deviation, and the different green shaded lines are the linear trends of mean frequencies in each RCM respectively. The mean frequency of hot summer days, averaged over the multi-model RCM ensemble (excluding TSMP), is shown with the solid blue line, and its linear trend is shown with the dashed blue line.~~ (e.g., Koster et al., 2009; Seneviratne et al., 2010; Jach et al., 2022).

~~In order to evaluate the impact of groundwater coupling on the interannual variability of hot summer days in RCMs, we examine the mean frequency of hot summer days in Europe in the ensemble of the EURO-CORDEX climate change scenario RCM control runs (see Table 1) from 1976 to 2005, with regard to the reference period 1961-1990 in each RCM (Fig. 3; see Sect. 2.4 for definitions). We calculate the mean frequency of hot summer days as the TG90p index, averaged over the total number of days during the summer season (92 days) and spatially averaged within all land-pixels of the focus domain (see Fig. 2). Comparison of the mean frequency of hot summer days from TSMP and individual RCMs, as well as the RCM multi-model mean, suggests that groundwater coupling does not seem to have a systematic impact on the occurrence of hot days. The interannual variability of summer heat events is strongly controlled by the large-scale atmospheric circulation imposed by the boundary conditions (see also Vautard et al., 2013a). Thus the distribution of hot summer days largely depends on the driving GCMs.~~

~~In Europe, an increasing linear trend of the frequency of hot summer days averaged over the focus domain is observed in all RCMs of the considered EURO-CORDEX ensemble (see Fig. 3). The frequency averaged over the multi-model RCM ensemble grows by about 1.5 times from 1976 to 2005 (dashed blue line in Fig. 3). The TSMP simulation gives the lowest linear trend of the frequency of hot summer days averaged over the focus domain in the considered EURO-CORDEX ensemble (dashed red line in Fig. 3). From the extrapolation functions shown in Fig. 3, the mean frequency of summer hot days in Europe is about 10%~~

~~smaller in TSMP than in the RCM ensemble mean in 2005. Most RCMs in the considered EURO-CORDEX ensemble show an increasing linear trend also in individual PRUDENCE regions (Fig. **??**). There are many studies that point to an increasing trend in the number of hot days worldwide: while the trend was not significant from 1950s until 1990s, it accelerates starting from 1990s and is associated with global warming (e.g., Frich et al., 2002; Perkins et al., 2012; Lhotka et al., 2018; Lorenz et al., 2019; Perkins-~~

3.2 ~~Influence of groundwater on the occurrence of heat events of different duration~~

3.2 Heat events of different durations

The average summer seasonal number of heat events (i.e., a series of consecutive hot days) of different duration that occur in the focus domain between 1976 and 2005 is presented in Fig. 7a. The total number of heat events per land grid element of the focus domain varies between 4.18 in COSMO-crCLIM driven by CNRM-CM5 and 4.86 in REMO2015 driven by NCC-NorESM1-M. The ratio of the number of heat events between CORDEX RCMs and TSMP (blue lines in Fig. 7a) increases towards heat events of long durations ($\geq$6 days), i.e., heat waves, and indicates that TSMP systematically simulates the least number of heat waves compared to the CORDEX ensemble. REMO RCMs tend to simulate more heat waves with long durations than COSMO RCMs.

Different GCM-RCMs simulate different spatial distributions of heat waves, whereas TSMP produces again the smoothest distribution of the decadal number of heat waves compared to the CORDEX ensemble, resulting in the least regional differences (Fig. 8). The number of heat waves over a decade in the focus domain ranges from the lowest value of 3.25 in TSMP driven by MPI-ESM-LR, to the highest of 5.09 in REMO2015 driven by IPSL-CM5A-LR (Fig. B1 in Appendix B). Comparing TSMP with CORDEX MPI-driven RCMs, CORDEX RCMs driven by MPI-ESM-LR simulate the highest number of heat waves toward Southern Europe, while in TSMP the most heat waves are located in Central Europe (see Fig. 8a-d). Strong differences between TSMP and the CORDEX MPI-driven RCMs appear over the Iberian Peninsula and the Mediterranean, and the smallest differences are in Scandinavia (see Fig. B1 in Appendix B). TSMP simulates fewer heat waves in all PRUDENCE regions except Mid-Europe, compared to the most compatible available CORDEX RCM, CCLM forced by MPI-ESM-LR.

~~In this sub-section, we assess the impact of groundwater coupling on the duration of heat events in Europe. The annual number of heat events that occur on average per land grid point of the focus domain~~

The contribution of heat waves to the total number of hot days during the summer season ~~between 1976 and 2005 as a function of the duration of these heat events is shown in~~ varies among GCM-RCMs (Fig. ~~7a. The ratio of the number of heat events suggests that groundwater coupling systematically impacts the duration of heat events in the simulations (presented with different types of blue lines in~~ 9). Heat waves account from 22.38 % of hot days in TSMP driven by MPI-ESM-LR to 34.40 % in REMO2015 driven by IPSL-CM5A-LR, on average in the focus domain (Fig. ~~7a). In TSMP, the mean number~~ B2 in Appendix B). Therefore, the proportion of heat events ~~with a duration exceeding 2 days is systematically smaller compared to the RCMs of the considered EURO-CORDEX ensemble. In particular, the average number of heat waves (duration>6days), is 1.5-8 times lower. In addition, there is a small increase in the number of single-day heat events~~ that do not belong to heat waves

is higher in TSMP compared to the CORDEX ensemble. Note that, for example, Vautard et al. (2013a), Plavcová and Kyselý (2016) have previously found a systematic tendency of most RCMs to overestimate the number and duration of long heat waves in comparison to observations.

The lowest annual number of summer heat events per land-pixel within the PRUDENCE regions is found in Scandinavia, reaching about 3.9 heat events (, indicating that TSMP generates more heat events with a duration of fewer than 6 days. Scandinavia is the region with the largest contribution of heat waves to the total number of hot days, on average in the considered RCM ensemble, which is expected to coincide with the region with the highest number of heat waves (see Fig. ??). Compared to the RCMs of the considered EURO-CORDEX ensemble, TSMP systematically simulates fewer heat waves in all PRUDENCE regions except the British Isles. The strongest effect of groundwater coupling on buffering heat waves is observed 8). Eastern Europe is the region with the least number of heat waves and the smallest contribution of heat waves to the total number of hot days. The largest discrepancy between TSMP and the CORDEX RCMs driven by the MPI-ESM-LR appear in the Iberian Peninsula , France, and the Alps; heat waves with a duration >12 days occur even 10-20 times less often in TSMP compared to the CORDEX ensemble. and the Mediterranean.

Different responses to groundwater coupling in different PRUDENCE regions may be explained by the soil moisture-temperature feedback associated with the different evaporative regimes, energy-limited (predominant in Scandinavia and Northeastern Europe) versus moisture-limited (Southern and Southeastern Europe) (e.g., Koster et al., 2009; Knist et al., 2017; Haghighi et al., 2018; Jac .

3.3 Groundwater impact on the intensity of heat Heat waves and the corresponding frequencyof different intensities

In this sub-section, we focus on heat waves, i.e. heat events with a duration exceeding 6 days. The dependency The dependence of the frequency of heat waveson their , which occurred between 1976 and 2005 in the focus domain, on the intensity is shown in Fig. 7b, see also Sect. 2.4 for definitions. The heat wave frequency presented in Fig. 7b describes the fraction . The maximum frequency of heat waves of a certain intensity that occurred during the 30-year summer periods from 1976 to 2005 in the focus domain in each RCM. The maximum frequency is equal to 1 for the intensity larger an intensity greater than 0 because all heat waves are taken into account for every RCM. From the ratio of heat wave frequencies of RCMs to TSMP (shown with different types of each RCM. The ratio of the frequency of heat waves between CORDEX RCMs and TSMP (blue lines in Fig. 7b) , we note a quite large spread of heat wave frequencies in the EURO-CORDEX ensemble, which increases towards heat waves of high intensity. TSMP exhibits increases toward intense heat waves (≥5 K). It shows a systematic behavior with fewer heat waves of high intensity of TSMP to simulate less intense heat waves on average in the focus domain compared to the CORDEX ensemble: the frequency of high-intensity heat waves is up to . The largest discrepancy is found between TSMP and CCLM driven by MPI-ESM-LR (blue solid line in Fig. 7b), up to a factor of 12 times lower in TSMP . Our results also indicate that groundwater coupling has a stronger impact or even more, depending on the intensity of considered. The REMO RCM, driven by different GCMs, shows the smallest differences to TSMP, while REMO2015 driven by IPSL-CM5A-LR simulates even less intense heat waves than on their duration in the TSMPsimulations (see the ratio between CCLM-MPI and TSMP in TSMP. Overall, COSMO RCMs tend to simulate more intense heat waves than REMO RCMs.

The spatial distribution of the intense heat waves differs between GCM-RCMs, with their highest frequency in France and Scandinavia and the lowest in the Alps, on average in the CORDEX ensemble (Fig. ~~7a, b). Previously, Vautard et al. (2013a) and Furusho-Percot et al. (2022) have shown that RCMs tend to overestimate the intensity of heat events, as well as the frequency of high-intensity heat waves .~~

~~The~~ 10, Fig. B3 in Appendix B). Note that the frequency ~~of~~ is defined in relation to the total number of heat waves in each RCM. The mean frequency of intense heat waves in ~~different PRUDENCE regions has a different response to groundwater coupling in the simulations (Fig. **??**).The response is almost negligible in Scandinavia, with good agreement between RCMs of the EURO-CORDEX ensemble, while it is significant in other PRUDENCE regions (e.g. , Iberian Peninsula, France, Mid-Europe, Mediterranean, Eastern Europe) with a spread in the frequency of high-intensity heat waves of 20 times or more. The predominance of the energy-limited evaporative regime in Scandinaviaand Northern Europe leads to a weaker land-atmosphere coupling, and thus to a relatively low impact of groundwater coupling on the frequency of simulated heat waves of high intensity.~~ the focus domain ranges from the lowest value of 0.174 in REMO2015 driven by IPSL-CM5A-LR to the highest of 0.301 in CCLM driven by MPI-ESM-LR, i.e., 17.4-30.1 % of all simulated heat waves exceed the intensity of 5 K. Compared to CCLM driven by MPI-ESM-LR, TSMP simulates a lower frequency of intense heat waves in all PRUDENCE regions except Scandinavia. The largest discrepancies and the highest number of intense heat waves are in France, with TSMP simulating 24.6 % of all heat waves as intense and CCLM – 46.8 %, smallest differences are in Scandinavia, where TSMP simulates 19.3 % of all heat waves as intense and CCLM – 17.5 %. It is important to note that the regions with the highest number of heat waves do not necessarily coincide with the regions with the highest number of intense heat waves (see Fig. 8 and Fig. 10). The origin of these differences should be further investigated and is beyond the scope of this analysis.

4 Summary and conclusions

In this study, we presented, in the context of dynamical downscaling of GCMs with RCMs experiment for climate change studies, a first-of-its-kind TSMP dataset forced by the CMIP5 MPI-ESM-LR GCM boundary conditions, where 3D groundwater hydrodynamics were explicitly represented. We studied the impact of groundwater ~~on summer~~ coupling on the statistics of simulated heat events in ~~a new dataset from a coupled regional climate system, the Terrestrial Systems Modelling Platform (TSMP), with an explicit representation of three-dimensional groundwater hydrodynamics, compared to an~~ regional historical climate simulations, with potential implications for climate change projections, by comparing TSMP results with the ensemble of EURO-CORDEX climate change scenario RCM control runs driven as well by CMIP5 GCMs. In particular, we investigated the ~~impact of groundwater coupling on the frequency~~ number of hot days ~~, the occurrence of heat events of different duration, and the frequency of high-intensity heat waves in Europe~~ and heat waves of different durations and intensities in Europe during the summer season between 1976 and 2005 ~~with respect~~ relative to the reference period 1961-1990 in each RCM.

Our ~~results show that the impact of groundwater coupling on the frequency of hot days during the summer season, generally, depends on the time and region under consideration. There is an increasing trend in the frequency of hot summer days in Europe in all RCMs of the considered ensemble, whereas TSMP is the lowest. We found that the explicit representation of groundwater in RCMs leads to fewer simulated severe heat events. TSMP systematically shows a lower number of heat events lasting 6 or~~

~~more days , so-called heat waves,~~ analysis shows that TSMP simulates heat events consistently with the EURO-CORDEX ensemble, although there are statistical differences and we relate these to groundwater coupling. TSMP simulates lower means as well as a lower interannual variability in the number of hot days on average in Europe~~; it is by about 1.5-8 times less than in~~ , compared to the CORDEX ensemble. ~~In addition, TSMP simulates a slightly higher number of single-day summer heat events~~ The decadal change in the number of hot days over Europe in TSMP is also lower compared to the CORDEX ensemble ~~. The frequency of high-intensity heat waves is also lower in TSMP on average in Europe, up to 12 times,~~ average. TSMP systematically simulates fewer heat waves and tends to simulate less intense heat waves compared to the ~~CODEX ensemble. The local impact of explicit groundwater representation in RCMs is linked to different evaporative regimes and , thus, regions with different strengths of land-atmosphere coupling. We found a smaller impact of groundwater coupling on the extreme heat event characteristics in regions with an energy-limited regime (e.g., British Isles and Scandinavia), and a stronger impact in regions with moisture-limited regime (Southern and Southeastern Europe), which is intuitive.~~ CORDEX ensemble. The most sensitive regions to groundwater coupling appear to be the Iberian Peninsula and the Mediterranean, while Scandinavia is the least sensitive.

From a comparison of TSMP and CCLM driven by MPI-ESM-LR, with the largest differences in the COSMO lower boundary condition accounting for groundwater feedbacks in TSMP, we found that TSMP in the considered focus domain covering Europe simulates on average lower:

- mean number of hot days (TSMP – 10.95 days, CCLM – 11.80 days);
- variability of the number of hot days (TSMP – 6.80 days, CCLM – 8.33 days);
- decadal change in the number of hot days (TSMP – 1.53 days, CCLM – 1.86 days);
- decadal number of heat waves (TSMP – 3.25, CCLM – 3.78);
- contribution of heat waves to the number of hot days (TSMP – 22.38 %, CCLM – 24.96 %);
- frequency of intense heat waves (TSMP – 0.193, CCLM – 0.301).

This study clearly indicates that a coupled regional climate system with a closed terrestrial water cycle, such as TSMP, systematically simulates a different climatology of ~~extreme heat events~~ heat event compared to uncoupled RCMs~~of the EURO-CORDEX ensemble. The results emphasize the importance of groundwater coupling for simulating extreme heat events. Explicit representation of~~ . The explicit representation of subsurface hydrodynamics and groundwater in RCMs may be ~~a key for bias reduction in the occurrence~~ key for the reduction of biases in the simulated duration and intensity of heat waves, particularly in Southern Europe. In the future, this work will be extended to investigate ~~regional climate projections and, in particular, the evolution of extreme~~ the evolution of heat events under different climate change scenarios in TSMP compared to uncoupled RCMs and their control simulations.

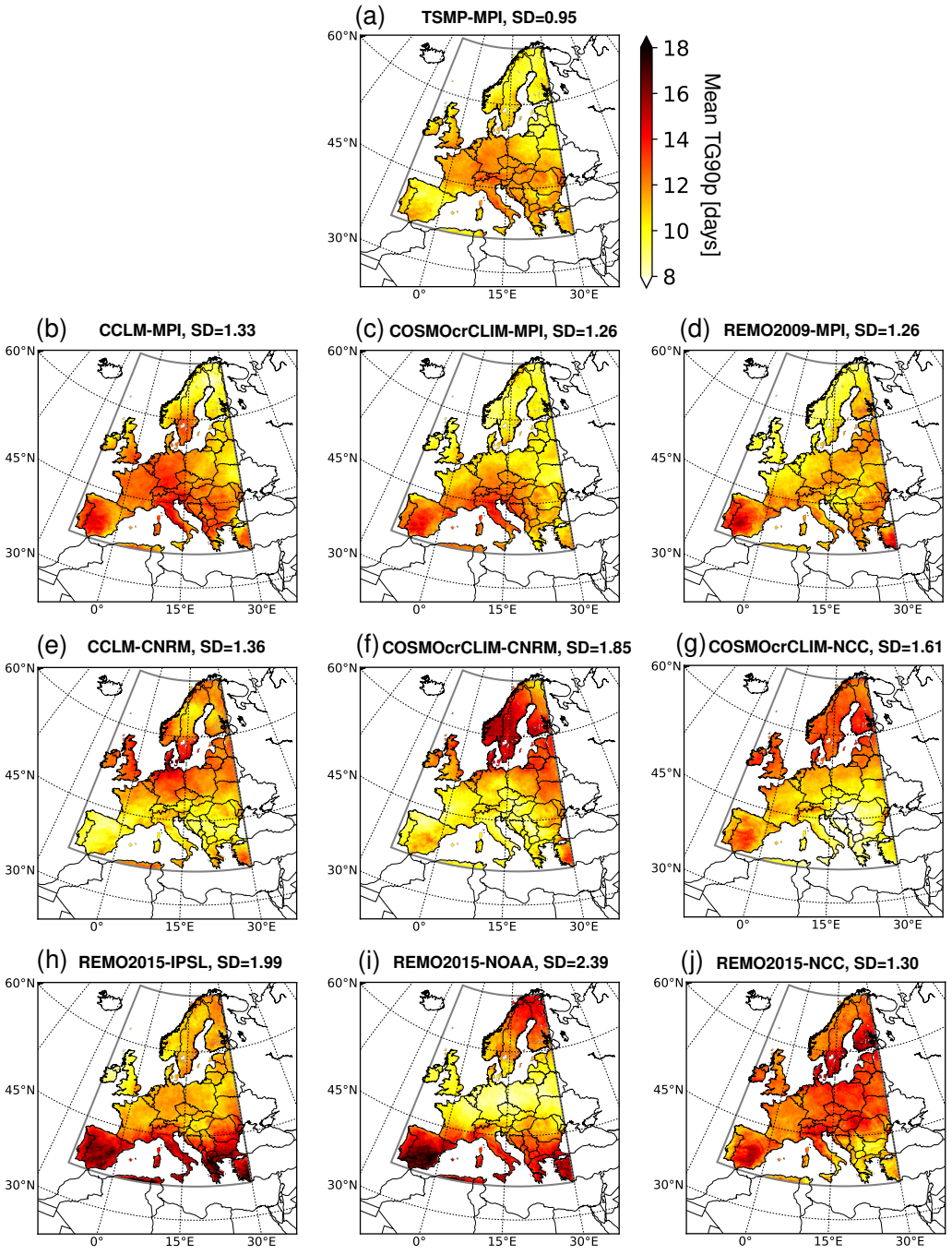

Figure 4. Spatial distribution of the number of hot days (TG90p index) averaged between 1976 and 2005 with respect to the reference period 1961-1990 for the summer season, in the ensemble of EURO-CORDEX climate change scenario RCM control runs. The standard deviation (SD) of the spatial distribution is also indicated on each figure.

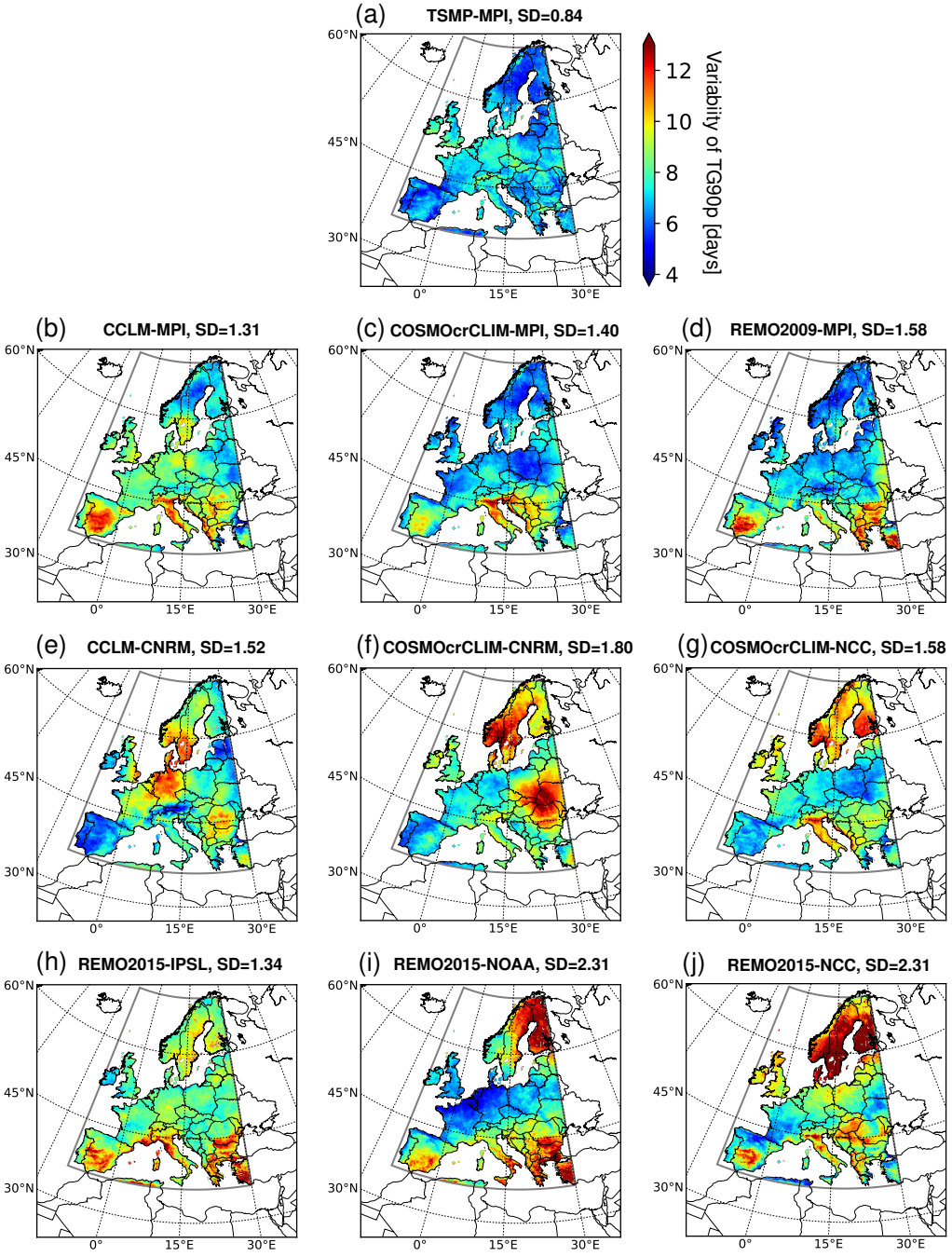

Figure 5. Variability of the hot days number (TG90p index) for the summer season, calculated for each land grid element as the standard deviation of TG90p between 1976 and 2005, in the ensemble of EURO-CORDEX climate change scenario RCM control runs. The standard deviation (SD) of the spatial distribution is also indicated on each figure.

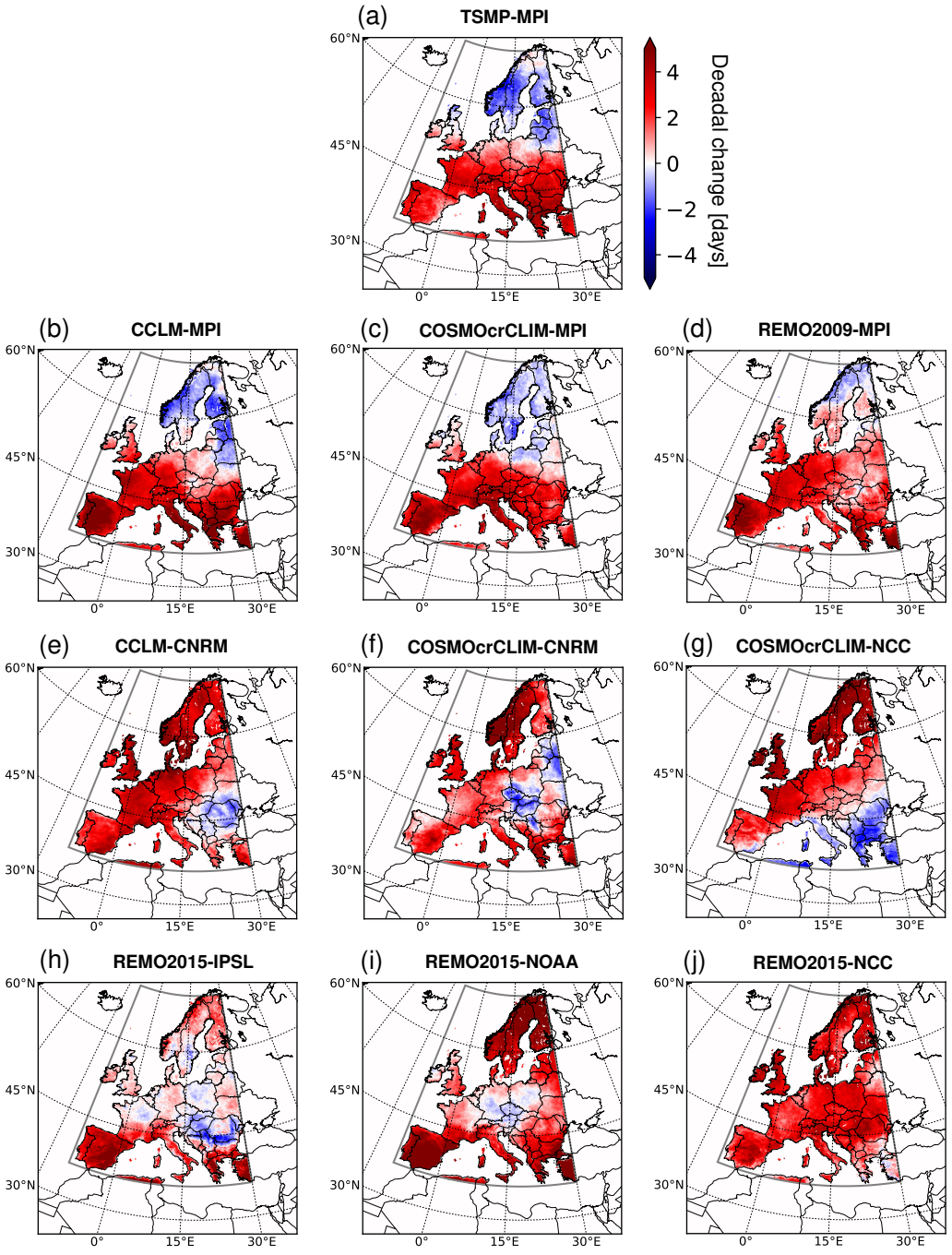

Figure 6. Spatial distribution of the decadal change in the number of hot summer days (TG90p index), based on data from 1976 to 2005 with respect to the reference period 1961-1990, in the ensemble of EURO-CORDEX climate change scenario RCM control runs. Decadal change is calculated as a linear trend for every land grid element.

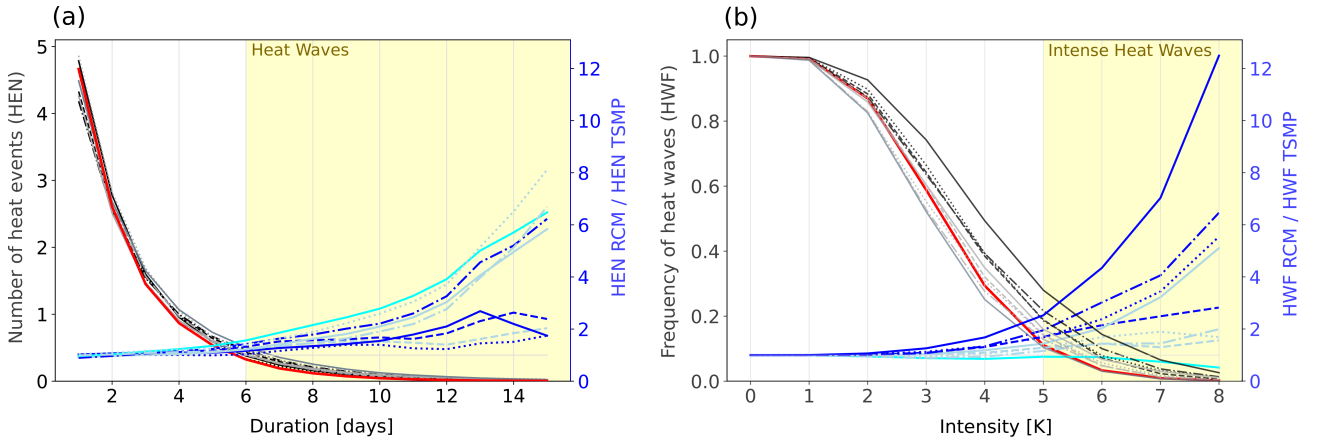

RCM-GCM	Total HEN per land pixel
TSMP-MPI	4.66
CCLM-MPI	4.79
CCLM-CNRM	4.33
COSMO-crCLIM-MPI	4.62
COSMO-crCLIM-CNRM	4.18
COSMO-crCLIM-NCC	4.26
REMO2009-MPI	4.49
REMO2015-NCC	4.86
REMO2015-NOAA	4.63
REMO2015-IPSL	4.49

Figure 7. (a) Average number of ~~summer~~ heat events (HEN, y-axis) of duration equal or larger than a given number of days (x-axis) as a function of this number of days~~(a)~~; the averaging is performed over the total number of ~~land-pixels~~ land grid elements of the focus domain ~~(see Fig. 2)~~ and ~~the total number of~~ 30 years, from 1976 to ~~2005~~ 2005. (~~30 years~~b) ~~.~~ Frequency of heat waves (HWF, y-axis) with an intensity higher or equal than a given value in abscissa occurring in the focus domain ~~during the summer seasons,~~ from 1976 to 2005 as a function of this intensity~~(b)~~. The panels also show the ratio of ~~quantities~~ HEN and HWF from RCMs ~~to~~ and TSMP. Data are taken from the summer seasons between 1976 and 2005 with respect to the reference period 1961-1990 in each RCM of the CORDEX ensemble. The representation of the dependencies is adopted from the work of Vautard et al. (2013a).

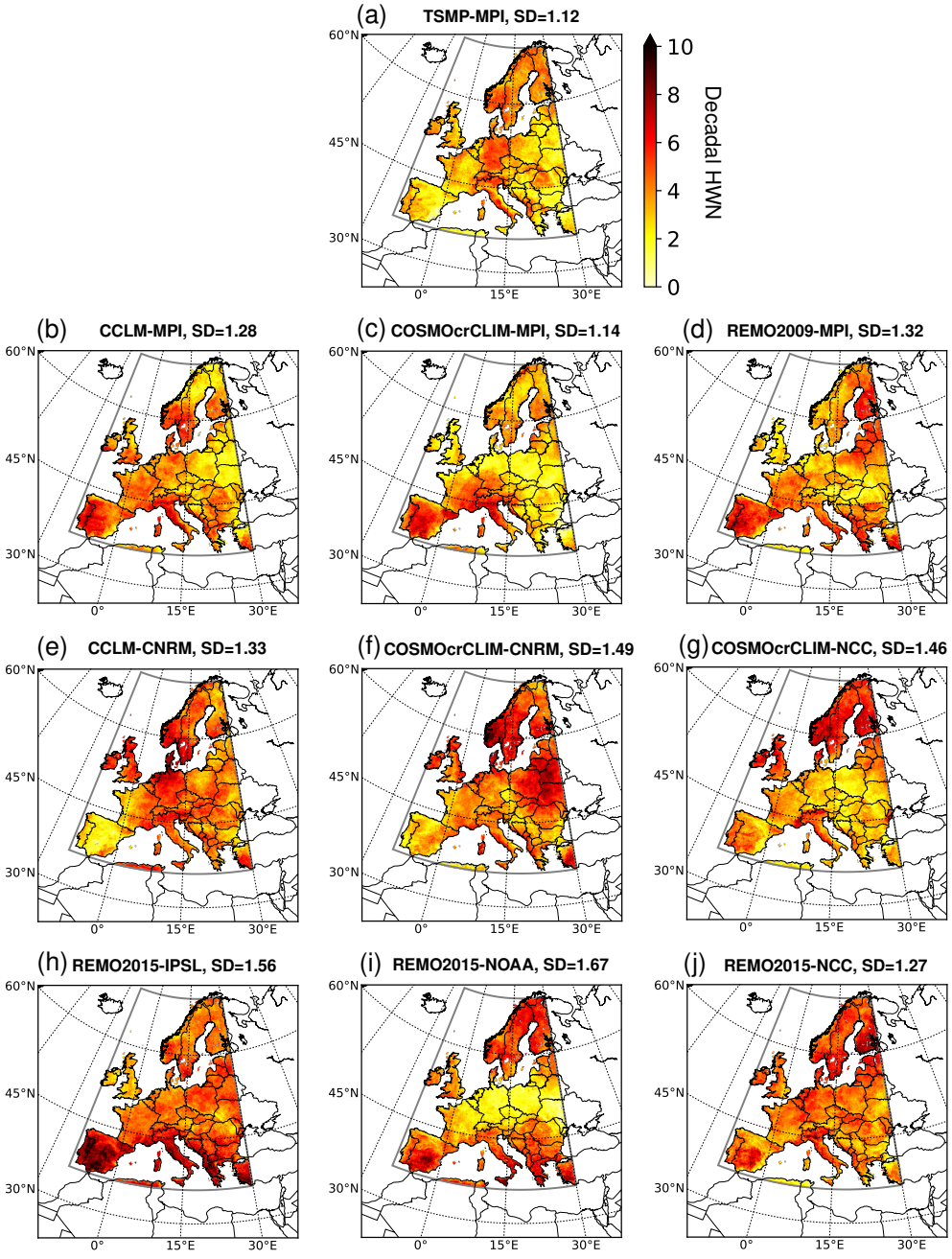

Figure 8. Spatial distribution of the heat waves number (HWN) over a decade based on data from 1976 to 2005 with respect to the reference period 1961-1990, in the ensemble of EURO-CORDEX climate change scenario RCM control runs (see Table 1)~~, represented with different colours and lines in the plots~~. The standard deviation is also indicated above each figure.

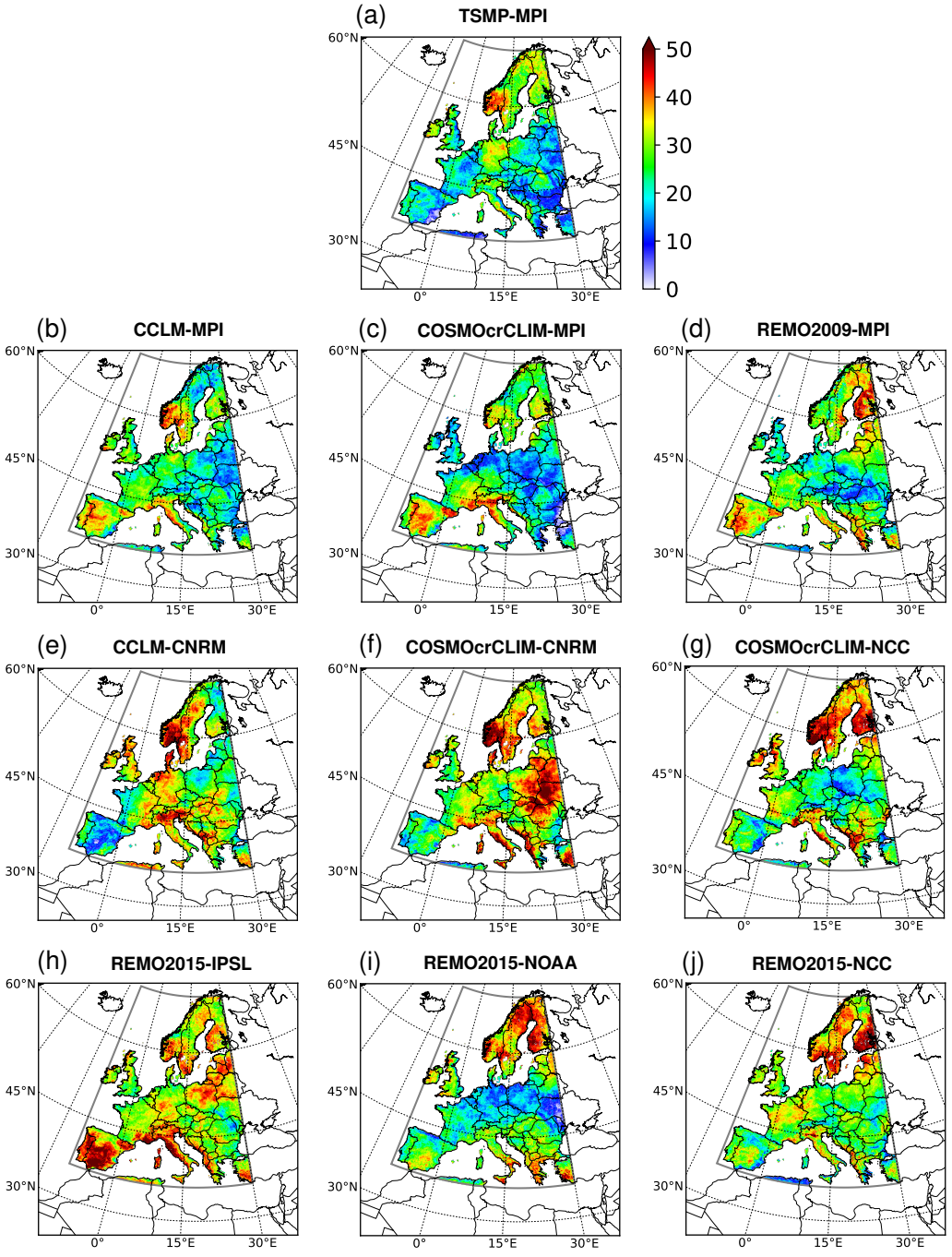

Figure 9. Contribution of heat waves to the number of hot days [%], calculated from the number of hot days and heat waves accumulated between 1976 and 2005, in the ensemble of EURO-CORDEX climate change scenario RCM control runs.

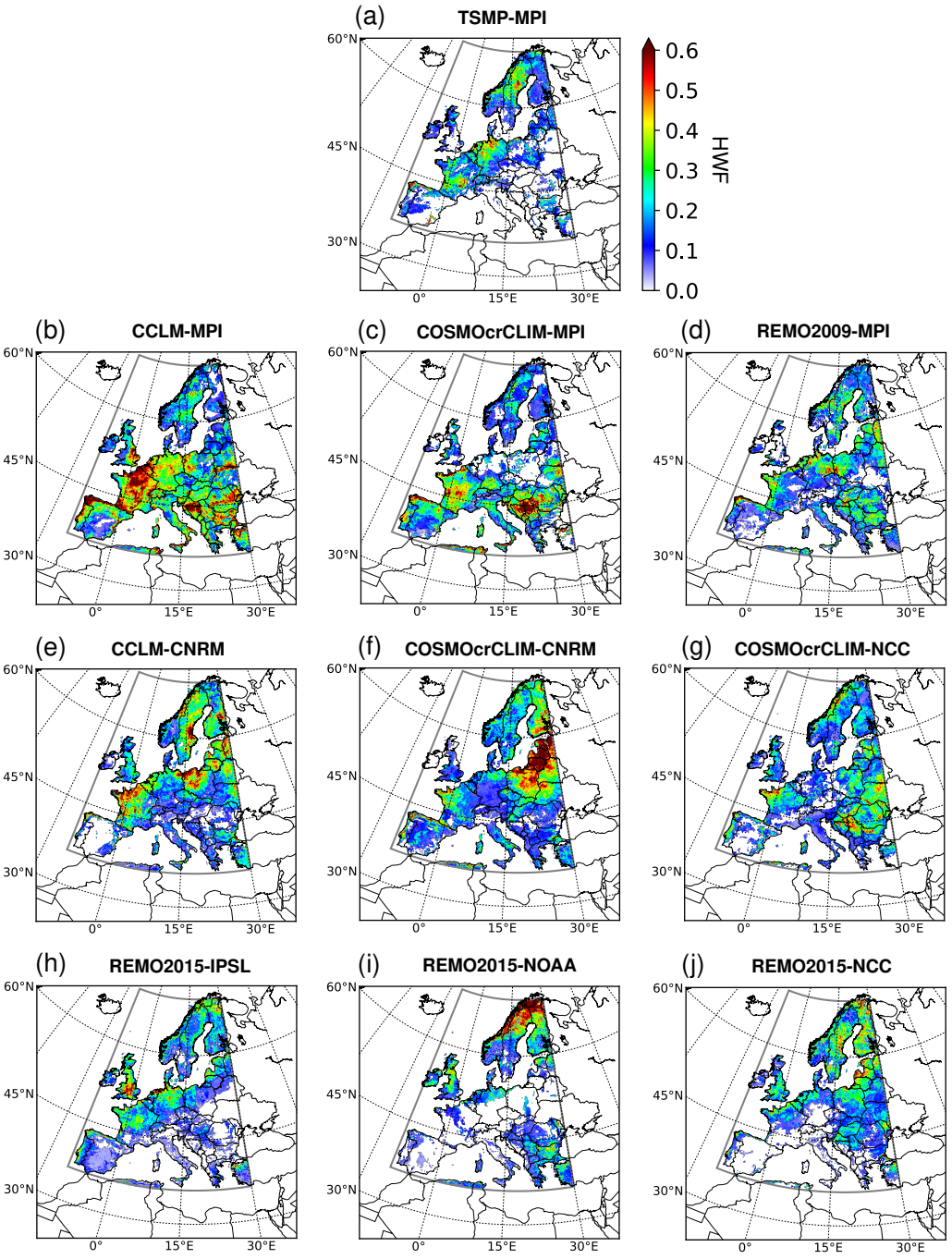

Figure 10. Frequency of heat waves (HWF) with an intensity above 5 K occurring between 1976 and 2005 with respect to the reference period 1961-1990, in the ensemble of EURO-CORDEX climate change scenario RCM control runs.

Appendix A: ~~Impact~~ Number of ~~groundwater coupling on the heat events frequency, duration and intensity~~ hot days for ~~PRUDENCE~~ different regions

~~Time series of the mean frequency~~

RCMs \ Regions	BI	IP	FR	ME	SC	AL	MD	EA	FD
TSMP-MPI	10.95	10.36	11.50	11.76	10.00	12.20	11.40	11.13	10.95
CCLM-MPI	11.49	12.64	12.46	12.80	10.42	13.27	12.62	11.50	11.80
COSMO-crCLIM-MPI	9.94	12.54	11.28	11.18	9.93	12.91	12.03	10.82	11.10
REMO2009-MPI	9.45	12.75	10.82	10.90	10.24	11.56	11.59	11.28	11.14
CCLM4-CNRM	12.89	9.66	10.93	12.62	12.06	10.74	10.49	11.16	11.32
COSMO-crCLIM-CNRM	12.05	10.14	9.87	10.87	13.87	10.15	9.85	11.26	11.46
COSMO-crCLIM-NCC	12.78	11.66	11.21	10.96	12.84	10.76	9.02	9.91	11.10
REMO2015-NCC	12.61	12.89	12.06	12.86	13.31	13.27	11.27	12.95	12.72
REMO2015-IPSL	9.56	15.00	11.45	11.48	11.29	12.64	15.25	11.63	12.38
REMO2015-NOAA	9.96	15.33	10.54	8.98	12.21	11.56	13.87	10.05	11.77

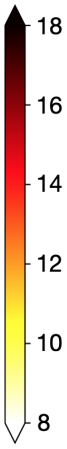

Figure A1. Mean number of hot ~~summer~~ days, i.e., TG90p index, [days] for the summer season averaged between 1976 and ~~its linear trends during 1976-2005~~ 2005 with respect to the reference period 1961-1990 ~~,~~ in the ensemble of EURO-CORDEX climate change scenario RCM control runs ~~(see Table 1)~~ for ~~PRUDENCE regions. Shown frequencies are calculated as the TG90p index, averaged over~~ the ~~total number of days during the summer season~~ focus domain (~~92 days~~FD) and ~~spatially averaged over all land-pixels in each PRUDENCE region. The solid and dashed red lines show~~ the ~~mean frequency of hot days in summer from TSMP simulation~~PRUDENCE regions: British Isles (BI), ~~as well as its linear trend. The black and grey lines represent the other RCMs' frequencies of hot days~~Iberian Peninsula (IP), ~~the shaded blue area represents their standard deviation~~France (FR), ~~and the different green tone lines are the linear trends. The mean frequency of hot summer days~~Mid-Europe (ME), ~~averaged over the multi-model RCM ensemble~~ Scandinavia (~~excluding TSMP~~SC), ~~and its linear trend is shown with the solid and dashed blue lines.~~

~~Average number of heat events~~ Alps (~~NHE~~AL)~~of duration equal to or larger than a given number of days~~ , Mediterranean (~~shown on X-axis~~MD)~~as a function of this number of days for PRUDENCE regions. The averaging is performed over the total number of land-pixels within every PRUDENCE region~~ , Eastern Europe (EA); see Fig. ~~2) and the total number of~~ 4 for the ~~investigated years from 1976 to 2005 (30 years)~~spatial distribution.~~Solid red lines show the resulting average number~~

~~Frequency of heat waves (FHW) with an intensity equal to or greater than a given value in abscissa occurring~~

Appendix B: Heat waves characteristics for different regions

RCMs \ Regions	BI	IP	FR	ME	SC	AL	MD	EA	FD
TSMP-MPI	7.68	6.17	6.92	7.43	6.26	7.50	6.93	6.93	6.80
CCLM-MPI	8.50	9.59	8.30	8.53	7.45	8.82	9.34	8.02	8.33
COSMO-crCLIM-MPI	6.75	8.01	6.56	6.90	6.56	8.56	9.00	7.42	7.38
REMO2009-MPI	6.73	8.94	7.36	6.81	6.48	7.39	9.37	7.62	7.62
CCLM4-CNRM	8.07	6.37	8.72	10.00	8.47	7.32	8.28	8.17	8.21
COSMO-crCLIM-CNRM	8.50	6.84	7.38	7.42	10.22	8.38	8.19	10.31	8.90
COSMO-crCLIM-NCC	9.24	6.89	7.91	7.41	10.06	8.73	8.79	7.59	8.37
REMO2015-NCC	9.94	8.05	7.21	8.57	12.21	8.48	8.86	8.77	9.42
REMO2015-IPSL	7.74	9.51	8.16	8.39	8.94	9.60	10.13	8.40	8.97
REMO2015-NOAA	6.88	8.71	6.18	5.87	10.24	8.05	10.49	8.11	8.69

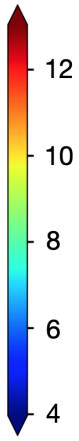

Figure A2. Variability of ~~heat events from the TSMP simulations. To improve readability,~~ the ~~average~~ hot days number~~of heat events from RCMs is not shown on the sub-figures, instead we present the ratio of RCMs to TSMP with blue lines of different types~~i.~~Data are taken from~~ e., TG90p index, [days] for the summer season ~~between~~ from 1976 ~~and~~ to 2005 with respect to the reference period 1961-1990 in ~~each RCM of~~ the ensemble of EURO-CORDEX climate change scenario RCM control runs for the focus domain (FD) and the PRUDENCE regions: British Isles (BI), Iberian Peninsula (IP), France (FR), Mid-Europe (ME), Scandinavia (SC), Alps (AL), Mediterranean (MD), Eastern Europe (EA); see ~~Table~~Fig. ~~1)~~4 for the spatial distribution.

RCMs \ Regions	BI	IP	FR	ME	SC	AL	MD	EA	FD
TSMP-MPI	0.62	2.26	2.90	1.52	-0.98	3.33	3.74	1.84	1.53
CCLM-MPI	1.39	4.25	3.49	2.03	-0.89	3.29	4.40	1.21	1.86
COSMO-crCLIM-MPI	0.79	3.66	2.87	1.98	-0.62	4.02	2.86	1.47	1.68
REMO2009-MPI	1.80	3.69	3.29	2.67	0.15	2.50	2.65	1.29	1.88
CCLM4-CNRM	3.56	2.78	3.52	3.40	3.29	2.88	1.66	0.43	2.35
COSMO-crCLIM-CNRM	3.00	1.76	1.34	1.36	2.95	1.49	2.54	0.08	1.77
COSMO-crCLIM-NCC	4.50	1.58	3.56	2.43	4.09	1.32	-1.24	0.52	1.87
REMO2015-NCC	3.92	2.64	2.23	2.51	3.08	3.17	1.97	2.85	2.71
REMO2015-IPSL	0.55	3.89	0.57	0.23	0.87	1.27	2.22	-0.20	1.13
REMO2015-NOAA	1.11	5.18	1.44	0.13	4.27	1.27	3.49	1.16	2.68

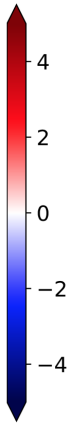

Figure A3. Decadal change in the ~~PRUDENCE regions during~~ number of hot days, i.e., TG90p index, [days] in the summer ~~seasons between~~ season, based on data from 1976 ~~and~~ to 2005 ~~as a function of this intensity. The intensity is calculated~~ with respect to the reference period 1961-1990, in ~~each RCM of~~ the ensemble of EURO-CORDEX climate change scenario RCM control runs for the focus domain (~~see Table 1~~FD) ~~. Solid red lines show the resulting frequency of heat waves from the TSMP simulations. To improve readability, the frequency of heat waves from RCMs is not shown on the sub-figures, instead we present~~ and the ~~ratio of RCMs to TSMP with different blue lines. Note that in some~~ PRUDENCE regions: British Isles (~~a~~BI), ~~g~~Iberian Peninsula (IP), ~~h~~France (FR), Mid-Europe (ME), Scandinavia (SC), Alps (AL), Mediterranean (MD), Eastern Europe (EA); see Fig. 6 for the ~~ratio of heat wave frequency of RCMs to TSMP ends before the range of abscissa because TSMP has zero values~~spatial distribution.

RCMs \ Regions	BI	IP	FR	ME	SC	AL	MD	EA	FD
TSMP-MPI	3.33	2.51	3.15	4.01	3.83	4.13	3.04	2.74	3.25
CCLM-MPI	3.85	4.88	4.20	3.84	3.59	4.50	4.48	2.86	3.78
COSMO-crCLIM-MPI	2.54	4.99	3.73	2.78	3.46	5.27	3.59	2.34	3.35
REMO2009-MPI	2.70	5.25	4.17	3.30	4.17	3.50	4.40	3.24	3.89
CCLM4-CNRM	5.25	2.53	3.57	5.31	4.69	5.09	4.43	4.15	4.31
COSMO-crCLIM-CNRM	4.84	3.18	3.69	4.09	5.65	4.03	4.18	5.27	4.63
COSMO-crCLIM-NCC	5.24	3.66	3.86	3.15	5.61	4.10	3.43	2.92	3.97
REMO2015-NCC	4.42	4.23	4.15	4.64	5.52	4.69	3.92	4.01	4.49
REMO2015-IPSL	3.21	7.25	4.49	4.23	4.44	5.59	6.77	4.58	5.09
REMO2015-NOAA	3.91	4.93	3.10	2.02	5.03	3.57	5.42	2.62	3.95

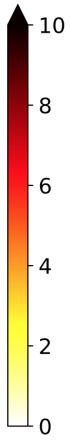

Figure B1. Decadal number of heat waves based on data from 1976 to 2005 with respect to the reference period 1961-1990, in the ensemble of EURO-CORDEX climate change scenario RCM control runs for the focus domain (FD) and the PRUDENCE regions: British Isles (BI), Iberian Peninsula (IP), France (FR), Mid-Europe (ME), Scandinavia (SC), Alps (AL), Mediterranean (MD), Eastern Europe (EA); see Fig. 8 for the spatial distribution.

RCMs \ Regions	BI	IP	FR	ME	SC	AL	MD	EA	FD
TSMP-MPI	25.36	17.47	19.62	25.61	29.87	24.40	19.33	17.79	22.38
CCLM-MPI	27.90	31.19	26.29	24.34	26.50	27.79	26.67	18.82	24.96
COSMO-crCLIM-MPI	18.78	31.96	25.50	18.49	27.59	33.62	24.46	16.27	23.46
REMO2009-MPI	21.81	33.04	28.35	22.39	32.63	23.50	30.18	21.92	27.22
CCLM4-CNRM	34.53	18.35	25.45	33.01	31.69	37.74	34.53	28.08	29.72
COSMO-crCLIM-CNRM	29.75	23.36	29.21	29.31	36.52	32.75	35.54	38.21	33.11
COSMO-crCLIM-NCC	34.70	23.94	30.71	23.12	39.04	30.05	33.07	23.70	29.61
REMO2015-NCC	30.16	25.39	32.05	29.06	38.37	29.72	27.54	26.69	30.20
REMO2015-IPSL	30.39	41.20	30.57	31.56	35.26	38.26	36.73	31.75	34.40
REMO2015-NOAA	30.77	25.20	21.41	16.51	37.52	24.58	32.54	19.36	26.97

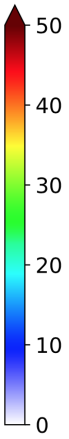

Figure B2. Contribution of heat waves to the number of hot days [%] during 1976-2005 with respect to the reference period 1961-1990, in the ensemble of EURO-CORDEX climate change scenario RCM control runs for the focus domain (FD) and the PRUDENCE regions: British Isles (BI), Iberian Peninsula (IP), France (FR), Mid-Europe (ME), Scandinavia (SC), Alps (AL), Mediterranean (MD), Eastern Europe (EA); see Fig. 9 for the spatial distribution.

RCMs \ Regions	BI	IP	FR	ME	SC	AL	MD	EA	FD
TSMP-MPI	0.118	0.189	0.246	0.233	0.193	0.145	0.171	0.148	0.193
CCLM-MPI	0.246	0.305	0.468	0.395	0.175	0.326	0.318	0.319	0.301
COSMO-crCLIM-MPI	0.181	0.246	0.361	0.216	0.152	0.213	0.262	0.318	0.241
REMO2009-MPI	0.173	0.156	0.207	0.230	0.211	0.125	0.180	0.218	0.202
CCLM4-CNRM	0.185	0.199	0.356	0.244	0.290	0.121	0.125	0.218	0.233
COSMO-crCLIM-CNRM	0.111	0.187	0.236	0.157	0.309	0.106	0.143	0.293	0.232
COSMO-crCLIM-NCC	0.160	0.188	0.234	0.163	0.193	0.105	0.165	0.268	0.204
REMO2015-NCC	0.181	0.173	0.163	0.166	0.267	0.082	0.123	0.184	0.205
REMO2015-IPSL	0.287	0.112	0.219	0.214	0.203	0.112	0.084	0.108	0.174
REMO2015-NOAA	0.213	0.094	0.120	0.197	0.294	0.101	0.144	0.141	0.213

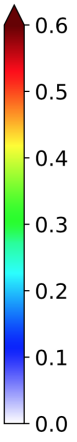

Figure B3. Frequency of heat waves with intensity exceeding 5 K based on data from 1976 to 2005 with respect to the reference period 1961-1990, in the ensemble of EURO-CORDEX climate change scenario RCM control runs for the focus domain (FD) and the PRUDENCE regions: British Isles (BI), Iberian Peninsula (IP), France (FR), Mid-Europe (ME), Scandinavia (SC), Alps (AL), Mediterranean (MD), Eastern Europe (EA); see Fig. 10 for the spatial distribution.

Code and data availability. The TSMP v1.2.2 used in this work is available through https://github.com/HPSCTerrSys/TSMP GIT repository. The dataset from the MPI-ESM-LR r1i1p1 GCM driven TSMP can be accessed at https://datapub.fz-juelich.de/slts/regional_climate_tsmp_hi-cam/ as open access research data.

Author contributions. The study was designed by S.K. with contributions by K.G., L.P-S., and N.W.. L.P.-S. performed the model simulations and data processing, N.W. provided technical and programming support, C.H. provided setups, configuration and workflow support. The analysis was conducted by L.P.-S. with further inputs from S.K. and K.G.. L.P.-S. wrote the manuscript. All co-authors contributed to the interpretation of the results, active discussions, and revisions of the paper. The work was done under the supervision of S.K..

Competing interests. The authors declare that they have no conflict of interest.

Acknowledgements. This work was funded by the Helmholtz Association of German Research Centres (HGF) under the HI-CAM project (Helmholtz Initiative Climate Adaptation and Mitigation) and by the German Ministry of Education and Research (Bundesministerium für Bildung und Forschung, BMBF) under the ClimXtreme project. We thank the EURO-CORDEX climate modelling groups for producing and making available their model output. We are grateful to the ~~Max-Plank~~ Max-Planck Institute for performing MPI-ESM-LR r1i1p1 GCM experiment and the German Climate Computing Centre (DKRZ) for providing the MPI-ESM-LR dataset. The authors gratefully acknowledge the Earth System Modelling Project (ESM) for funding this work by providing computing time on the ESM partition of the supercomputer JUWELS at the Jülich Supercomputing Centre (JSC) under the ESM project ID JIBG35. In addition, we thank the ~~Simulation and Data Laboratory Terrestrial Systems of the~~ Centre for High-Performance Scientific Computing in Terrestrial Systems (Geoverbund ABC/J, http://www.hpsc-terrsys.de) and the JSC for the computational support.

References

Alexander, L. V., Zhang, X., Peterson, T. C., Caesar, J., Gleason, B., Klein Tank, A. M. G., Haylock, M., Collins, D., Trewin, B., Rahimzadeh, F., Tagipour, A., Rupa Kumar, K., Revadekar, J., Griffiths, G., Vincent, L., Stephenson, D. B., Burn, J., Aguilar, E., Brunet, M., Taylor, M., New, M., Zhai, P., Rusticucci, M., and Vazquez-Aguirre, J. L.: Global observed changes in daily climate extremes of temperature and precipitation, J. Geophys. Res. Atmos., 111, D05109, https://doi.org/10.1029/2005JD006290, 2006.

Amengual, A., Homar, V., Romero, R., Brooks, H., Ramis, C., Gordaliza, M., and Alonso, S.: Projections of heat waves with high impact on human health in Europe, Glob. Planet. Change, 119, 71–84, https://doi.org/10.1016/j.gloplacha.2014.05.006, 2014.

Ashby, S. F. and Falgout, R. D.: A Parallel Multigrid Preconditioned Conjugate Gradient Algorithm for Groundwater Flow Simulations, Nucl. Sci. Eng., 124, 145–159, https://doi.org/10.13182/NSE96-A24230, 1996.

Baldauf, M., Seifert, A., Förstner, J., Majewski, D., Raschendorfer, M., and Reinhardt, T.: Operational Convective-Scale Numerical Weather Prediction with the COSMO Model: Description and Sensitivities, Mon. Weather Rev., 139, 3887–3905, https://doi.org/10.1175/MWR-D-10-05013.1, 2011.

Barlage, M., Tewari, M., Chen, F., Miguez-Macho, G., Yang, Z.-L., and Niu, G.-Y.: The effect of groundwater interaction in North American regional climate simulations with WRF/Noah-MP, Clim. Change, 129, 485–498, https://doi.org/10.1007/s10584-014-1308-8, 2015.

Barlage, M., Chen, F., Rasmussen, R., Zhang, Z., and Miguez-Macho, G.: The Importance of Scale-Dependent Groundwater Processes in Land-Atmosphere Interactions Over the Central United States, Geophysical Research Letters, 48, e2020GL092 171, https://doi.org/10.1029/2020GL092171, 2021.

Barriopedro, D., Fischer, E. M., Luterbacher, J., Trigo, R. M., and R., G.-H.: The Hot Summer of 2010: Redrawing the Temperature Record Map of Europe, Science, 332, 220–224, https://doi.org/10.1126/science.1201224, 2011.

Bellprat, O., Kotlarski, S., Lüthi, D., Elía, R. D., Frigon, A., Laprise, R., and Schär, C.: Objective Calibration of Regional Climate Models: Application over Europe and North America, Journal of Climate, 29, 819–838, https://doi.org/10.1175/JCLI-D-15-0302.1, 2016.

Bentsen, M., Bethke, I., Debernard, J. B., Iversen, T., Kirkevåg, A., Seland, Ø., Drange, H., Roelandt, C., Seierstad, I. A., Hoose, C., and Kristjánsson, J. E.: The Norwegian Earth System Model, NorESM1-M – Part 1: Description and basic evaluation of the physical climate, Geosci. Model Dev., 6, 687–720, https://doi.org/10.5194/gmd-6-687-2013, 2013.

Bosello, F., Roson, R., and Tol, R.: Economy-wide Estimates of the Implications of Climate Change: Sea Level Rise, Environ. Resource Econ., 37, 549–571, https://doi.org/10.1007/s10640-006-9048-5, 2007.

Campoy, A., Ducharne, A., Cheruy, F., Hourdin, F., Polcher, J., and Dupont, J. C.: Response of land surface fluxes and precipitation to different soil bottom hydrological conditions in a general circulation model, J. Geophys. Res. Atmos., 118, 10 725–10 739, https://doi.org/10.1002/jgrd.50627, 2013.

Christensen, J. H. and Christensen, O. B.: A summary of the PRUDENCE model projections of changes in European climate by the end of this century, Clim. Change, 81, 7–30, https://doi.org/10.1007/s10584-006-9210-7, 2007.

Christidis, N., Jones, G., and Stott, P.: Dramatically increasing chance of extremely hot summers since the 2003 European heatwave, Nature Clim. Change, 5, 46–50, https://doi.org/10.1038/nclimate2468, 2015.

Ciscar, J.-C., Iglesias, A., Feyen, L., Szabó, L., Van Regemorter, D., Amelung, B., Nicholls, R., Watkiss, P., Christensen, O. B., Dankers, R., Garrote, L., Goodess, C. M., Hunt, A., Moreno, A., Richards, J., and Soria, A.: Physical and economic consequences of climate change in Europe, Proc. Natl. Acad. Sci., 108, 2678–2683, https://doi.org/10.1073/pnas.1011612108, 2011.

Cornes, R. C., van der Schrier, G., van den Besselaar, E. J. M., and Jones, P. D.: An Ensemble Version of the E-OBS Temperature and Precipitation Data Sets, Journal of Geophysical Research: Atmospheres, 123, 9391–9409, https://doi.org/10.1029/2017JD028200, 2018.

Dee, D. P., Uppala, S. M., Simmons, A. J., Berrisford, P., Poli, P., Kobayashi, S., Andrae, U., Balmaseda, M. A., Balsamo, G., Bauer, P., Bechtold, P., Beljaars, A. C. M., van de Berg, L., Bidlot, J., Bormann, N., Delsol, C., Dragani, R., Fuentes, M., Geer, A. J., Haimberger, L., Healy, S. B., Hersbach, H., Hólm, E. V., Isaksen, L., Kallberg, P., Koehler, M., Matricardi, M., McNally, A. P., Monge-Sanz, B. M., Morcrette, J.-J., Park, B.-K., Peubey, C., de Rosnay, P., Tavolato, C., Thépaut, J.-N., and Vitart, F.: The ERA-Interim reanalysis: configuration and performance of the data assimilation system, Q. J. R. Meteorol. Soc., 137, 553–597, https://doi.org/10.1002/qj.828, 2011.

Déqué, M., Rowell, D. P., Lüthi, D., Giorgi, F., Christensen, J. H., Rockel, B., Jacob, D., Kjellström, E., de Castro, M., and van den Hurk, B.: An intercomparison of regional climate simulations for Europe: assessing uncertainties in model projections, Clim. Change, 81, 53–70, https://doi.org/10.1007/s10584-006-9228-x, 2007.

Déqué, M., Somot, S., Sanchez-Gomez, E., Goodess, C. M., Jacob, D., Lenderink, G., and Christensen, O. B.: The spread amongst ENSEMBLES regional scenarios: regional climate models, driving general circulation models and interannual variability, Clim. Change, 38, 951–964, https://doi.org/10.1007/s00382-011-1053-x, 2012.

Dirmeyer, P. A., Balsamo, G., Blyth, E. M., Morrison, R., and Cooper, H. M.: Land-Atmosphere Interactions Exacerbated the Drought and Heatwave Over Northern Europe During Summer 2018, AGU Advances, 2, e2020AV000283, https://doi.org/10.1029/2020AV000283, 2021.

Doms, G., Föorstner, J., Heise, E., Herzog, H.-J., Mironov, D., Raschendorfer, M., Reinhardt, T., Ritter, B., Schrodin, R., Schulz, J.-P., and Vogel, G.: Consortium for small-scale modelling: A description of the nonhydrostatic regional COSMO model. Part II: Physical parameterization, Tech. rep., https://doi.org/10.5676/DWD_pub/nwv/cosmo-doc_5.00_II, 2013.

Dufresne, J.-L., Foujols, M.-A., Denvil, S., and et al.: Climate change projections using the IPSL-CM5 Earth System Model: from CMIP3 to CMIP5, Clim. Dyn., 40, 2123–2165, https://doi.org/10.1007/s00382-012-1636-1, 2013.

Dunne, J. P., John, J. G., Adcroft, A. J., Griffies, S. M., Hallberg, R. W., Shevliakova, E., Stouffer, R. J., Cooke, W., Dunne, K. A., Harrison, M. J., Krasting, J. P., Malyshev, S. L., Milly, P. C. D., Phillipps, P. J., Sentman, L. T., Samuels, B. L., Spelman, M. J., Winton, M., Wittenberg, A. T., and Zadeh, N.: GFDL's ESM2 Global Coupled Climate–Carbon Earth System Models. Part I: Physical Formulation and Baseline Simulation Characteristics, J. Clim., 25, 6646–6665, https://doi.org/10.1175/JCLI-D-11-00560.1, 2012.

Duscher, K., Günther, A., Richts, A., Clos, P., Philipp, U., and Struckmeier, W.: The GIS layers of the "International Hydrogeological Map of Europe 1:1,500,000" in a vector format, Hydrogeol. J., 23, 1867–1875, https://doi.org/10.1007/s10040-015-1296-4, 2015.

Eltahir, E. A. B.: A Soil Moisture-Rainfall Feedback Mechanism: 1. Theory and observations, Water Resour. Res., 34, 765–776, https://doi.org/10.1029/97WR03499, 1998.

Erdenebat, E. and Tomonori, S.: Role of soil moisture-atmosphere feedback during high temperature events in 2002 over Northeast Eurasia, Prog. Earth. Planet. Sci., 5, 37, https://doi.org/10.1186/s40645-018-0195-4, 2018.

Espírito Santo, F., de Lima, M. I. P., Ramos, A. M., and Trigo, R. M.: Trends in seasonal surface air temperature in mainland Portugal, since 1941, Int. J. Climatol., 34, 1814–1837, https://doi.org/10.1002/joc.3803, 2014.

FAO: FAO/UNESCO Soil Map of the World, Revised Legend, with corrections and updates, World Soil Resources Report 60, FAO, Rome, https://www.fao.org/3/bl892e/bl892e.pdf, 1988.

Fernandez-Granja, J. A., Casanueva, A., Bedia, J., and Fernandez, J.: Improved atmospheric circulation over Europe by the new generation of CMIP6 earth system models, Clim. Dyn., 56, 3527–3540, https://doi.org/10.1007/s00382-021-05652-9, 2021.

Fernández, J., Frías, M. D., Cabos, W. D., Cofiño, A. S., Domínguez, M., Fita, L., Gaertner, M. A., García-Díez, M., Gutiérrez, J. M., Jiménez-Guerrero, P., Liguori, G., Montávez, J. P., Romera, R., and Sánchez, E.: Consistency of climate change projections from multiple global and regional model intercomparison projects, Clim. Dyn., 52, 1139–1156, https://doi.org/10.1007/s00382-018-4181-8, 2019.

Fischer, E. M. and Schär, C.: Consistent geographical patterns of changes in high-impact European heatwaves, Nat. Geosci., 3, 398–403, https://doi.org/10.1038/ngeo866, 2010.

Fischer, E. M., Seneviratne, S. I., Lüthi, D., and Schär, C.: Contribution of land-atmosphere coupling to recent European summer heat waves, Geophys. Res. Lett., 34, L06707, https://doi.org/10.1029/2006GL029068, 2007.

Frich, P., Alexander, L. V., Della-Marta, P., Gleason, B., Haylock, M., Klein Tank, A. M. G., and Peterson, T.: Observed coherent changes in climatic extremes during the second half of the twentieth century, Clim. Res., 19, 193–212, https://doi.org/10.3354/cr019193, 2002.

Friedl, M., McIver, D., Hodges, J., Zhang, X., Muchoney, D., Strahler, A., Woodcock, C., Gopal, S., Schneider, A., Cooper, A., Baccini, A., Gao, F., and Schaaf, C.: Global land cover mapping from MODIS: algorithms and early results, Remote Sens. Environ., 83, 287–302, https://doi.org/10.1016/S0034-4257(02)00078-0, the Moderate Resolution Imaging Spectroradiometer (MODIS): a new generation of Land Surface Monitoring, 2002.

Furusho-Percot, C., Goergen, K., Hartick, C., Kulkarni, K., Keune, J., and Kollet, S.: Pan-European groundwater to atmosphere terrestrial systems climatology from a physically consistent simulation, Sci. Data, 6, 320, https://doi.org/10.1038/s41597-019-0328-7, 2019.

Furusho-Percot, C., Goergen, K., Hartick, C., Poshyvailo-Strube, L., and Kollet, S.: Groundwater Model Impacts Multiannual Simulations of Heat Waves, Geophys. Res. Lett., 49, e2021GL096781, https://doi.org/10.1029/2021GL096781, 2022.

Gasper, F., Goergen, K., Shrestha, P., Sulis, M., Rihani, J., Geimer, M., and Kollet, S.: Implementation and scaling of the fully coupled Terrestrial Systems Modeling Platform (TerrSysMP v1.0) in a massively parallel supercomputing environment – a case study on JUQUEEN (IBM Blue Gene/Q), Geosci. Model Dev., 7, 2531–2543, https://doi.org/10.5194/gmd-7-2531-2014, 2014.

Giorgetta, M. A., Jungclaus, J., Reick, C. H., Legutke, S., Bader, J., Böttinger, M., Brovkin, V., Crueger, T., Esch, M., Fieg, K., Glushak, K., Gayler, V., Haak, H., Hollweg, H.-D., Ilyina, T., Kinne, S., Kornblueh, L., Matei, D., Mauritsen, T., Mikolajewicz, U., Mueller, W., Notz, D., Pithan, F., Raddatz, T., Rast, S., Redler, R., Roeckner, E., Schmidt, H., Schnur, R., Segschneider, J., Six, K. D., Stockhause, M., Timmreck, C., Wegner, J., Widmann, H., Wieners, K.-H., Claussen, M., Marotzke, J., and Stevens, B.: Climate and carbon cycle changes from 1850 to 2100 in MPI-ESM simulations for the Coupled Model Intercomparison Project phase 5, J. Adv. Model. Earth Syst., 5, 572–597, https://doi.org/10.1002/jame.20038, 2013.

Giorgi, F.: Thirty Years of Regional Climate Modeling: Where Are We and Where Are We Going next?, J. Geophys. Res. Atmos., 124, 5696–5723, https://doi.org/10.1029/2018JD030094, 2019.

Giorgi, F. and Coppola, E.: Does the model regional bias affect the projected regional climate change? An analysis of global model projections, Clim. Change, 100, 787–795, https://doi.org/10.1007/s10584-010-9864-z, 2010.

Giorgi, F. and Gutowski, W. J.: Regional Dynamical Downscaling and the CORDEX Initiative, Annu. Rev. Environ. Resour., 40, 467–490, https://doi.org/10.1146/annurev-environ-102014-021217, 2015.

Gleeson, T.: GLobal HYdrogeology MaPS (GLHYMPS) of permeability and porosity, Borealis, V1, https://doi.org/10.5683/SP2/DLGXYO, 2018.

Gleeson, T., Moosdorf, N., Hartmann, J., and van Beek, L. P. H.: A glimpse beneath earth's surface: GLobal HYdrogeology MaPS (GLHYMPS) of permeability and porosity, Geophys. Res. Lett., 41, 3891–3898, https://doi.org/10.1002/2014GL059856, 2014.

Grasselt, René and Schüttemeyer, D., Warrach-Sagi, K., Ament, F., and Simmer, C.: Validation of TERRA-ML with discharge measurements, Meteorol. Z., 17, 763–773, https://doi.org/10.1127/0941-2948/2008/0334, 2008.

Gutowski, W. J., Giorgi, F., Timbal, B., Frigon, A., Jacob, D., Kang, H.-S., Raghavan, K., Lee, B., Lennard, C., Nikulin, G., O'Rourke, E., Rixen, M., Solman, S., Stephenson, T., and Tangang, F.: WCRP COordinated Regional Downscaling EXperiment (CORDEX): a diagnostic MIP for CMIP6, Geosci. Model Dev., 9, 4087–4095, https://doi.org/10.5194/gmd-9-4087-2016, 2016.

Gutowski, W. J., Ullrich, P. A., Hall, A., Leung, L. R., O'Brien, T. A., Patricola, C. M., Arritt, R. W., Bukovsky, M. S., Calvin, K. V., Feng, Z., Jones, A. D., Kooperman, G. J., Monier, E., Pritchard, M. S., Pryor, S. C., Qian, Y., Rhoades, A. M., Roberts, A. F., Sakaguchi, K., Urban, N., and Zarzycki, C.: The Ongoing Need for High-Resolution Regional Climate Models: Process Understanding and Stakeholder Information, Bull. Am. Meteorol. Soc., 101, E664–E683, https://doi.org/10.1175/BAMS-D-19-0113.1, 2020.

Habeeb, D., Vargo, J., and Stone, B.: Rising heat wave trends in large US cities, Nat. Hazards, 76, 1651–1665, https://doi.org/10.1007/s11069-014-1563-z, 2015.

Haghighi, E., Short Gianotti, D. J., Akbar, R., Salvucci, G. D., and Entekhabi, D.: Soil and Atmospheric Controls on the Land Surface Energy Balance: A Generalized Framework for Distinguishing Moisture-Limited and Energy-Limited Evaporation Regimes, Water Resour. Res., 54, 1831–1851, https://doi.org/https://doi.org/10.1002/2017WR021729, 2018.

Hari, V., Rakovec, O., Markonis, Y., Hanel, M., and Kumar, R.: Increased future occurrences of the exceptional 2018-2019 Central European drought under global warming, Sci. Rep., 10, 12207, https://doi.org/10.1038/s41598-020-68872-9, 2020.

Hartick, C., Furusho-Percot, C., Goergen, K., and Kollet, S.: An Interannual Probabilistic Assessment of Subsurface Water Storage Over Europe Using a Fully Coupled Terrestrial Model, Water Resour. Res., 57, e2020WR027828, https://doi.org/https://doi.org/10.1029/2020WR027828, 2021.

Hartick, C., Furusho-Percot, C., Clark, M. P., and Kollet, S.: An Interannual Drought Feedback Loop Affects the Surface Energy Balance and Cloud Properties, Geophys. Res. Lett., 49, e2022GL100 924, https://doi.org/10.1029/2022GL100924, 2022.

Hawkins, E. and Sutton, R.: The Potential to Narrow Uncertainty in Regional Climate Predictions, Bull. Am. Meteorol. Soc., 90, 1095–1108, https://doi.org/10.1175/2009BAMS2607.1, 2009.

Horton, R. M., Mankin, J. S., Lesk, C., Coffel, E., and Raymond, C.: Review of Recent Advances in Research on Extreme Heat Events, Curr. Clim. Change. Rep., 2, 242–259, https://doi.org/10.1007/s40641-016-0042-x, 2016.

Iles, C. E., Vautard, R., Strachan, J., Joussaume, S., Eggen, B. R., and Hewitt, C. D.: The benefits of increasing resolution in global and regional climate simulations for European climate extremes, Geosci. Model Dev., 13, 5583–5607, https://doi.org/10.5194/gmd-13-5583-2020, 2020.

Ionita, M., Nagavciuc, V., Kumar, R., and Rakovec, O.: On the curious case of the recent decade, mid-spring precipitation deficit in central Europe, NPJ Clim. Atmos. Sci., 3, 49, https://doi.org/10.1038/s41612-020-00153-8, 2020.

Jach, L., Schwitalla, T., Branch, O., Warrach-Sagi, K., and Wulfmeyer, V.: Sensitivity of land–atmosphere coupling strength to changing atmospheric temperature and moisture over Europe, Earth Syst. Dynam., 13, 109–132, https://doi.org/10.5194/esd-13-109-2022, 2022.

Jacob, D. and Podzun, R.: Sensitivity studies with the regional climate model REMO, Meteorl. Atmos. Phys., 63, 119–129, https://doi.org/10.1007/BF01025368, 1997.

Jacob, D., Teichmann, C., Sobolowski, S., and et al.: Regional climate downscaling over Europe: perspectives from the EURO-CORDEX community, Reg. Environ. Change, 20, 51, https://doi.org/10.1007/s10113-020-01606-9, 2020.

Karl, T. R., Nicholls, N., and Ghazi, A.: Clivar/GCOS/WMO Workshop on Indices and Indicators for Climate Extremes Workshop Summary, Clim. Change, 42, 3–7, https://doi.org/10.1023/A:1005491526870, 1999.

Kautz, L.-A., Martius, O., Pfahl, S., Pinto, J. G., Ramos, A. M., Sousa, P. M., and Woollings, T.: Atmospheric blocking and weather extremes over the Euro-Atlantic sector – a review, Weather and Climate Dynamics, 3, 305–336, https://doi.org/10.5194/wcd-3-305-2022, 2022.

Keune, J., Gasper, F., Goergen, K., Hense, A., Shrestha, P., Sulis, M., and Kollet, S.: Studying the influence of groundwater representations on land surface-atmosphere feedbacks during the European heat wave in 2003, J. Geophys. Res. Atmos., 121, 13 301–13 325, https://doi.org/10.1002/2016JD025426, 2016.

Knist, S., Goergen, K., Buonomo, E., Christensen, O. B., Colette, A., Cardoso, R. M., Fealy, R., Fernández, J., García-Díez, M., Jacob, D., Kartsios, S., Katragkou, E., Keuler, K., Mayer, S., van Meijgaard, E., Nikulin, G., Soares, P. M. M., Sobolowski, S., Szepszo, G., Teichmann, C., Vautard, R., Warrach-Sagi, K., Wulfmeyer, V., and Simmer, C.: Land-atmosphere coupling in EURO-CORDEX evaluation experiments, J. Geophys. Res. Atmos., 122, 79–103, https://doi.org/10.1002/2016JD025476, 2017.

Kollet, S. J. and Maxwell, R. M.: Integrated surface–groundwater flow modeling: A free-surface overland flow boundary condition in a parallel groundwater flow model, Adv. Water. Resour., 29, 945–958, https://doi.org/10.1016/j.advwatres.2005.08.006, 2006.

Kollet, S. J. and Maxwell, R. M.: Capturing the influence of groundwater dynamics on land surface processes using an integrated, distributed watershed model, Water Resources Research, 44, https://doi.org/10.1029/2007WR006004, 2008.

Koster, R. D., Schubert, S. D., and Suarez, M. J.: Analyzing the Concurrence of Meteorological Droughts and Warm Periods, with Implications for the Determination of Evaporative Regime, J. Clim., 22, 3331–3341, https://doi.org/10.1175/2008JCLI2718.1, 2009.

Kuffour, B. N. O., Engdahl, N. B., Woodward, C. S., Condon, L. E., Kollet, S., and Maxwell, R. M.: Simulating coupled surface–subsurface flows with ParFlow v3.5.0: capabilities, applications, and ongoing development of an open-source, massively parallel, integrated hydrologic model, Geosci. Model Dev., 13, 1373–1397, https://doi.org/10.5194/gmd-13-1373-2020, 2020.

Lhotka, O. and Kyselý, J.: Characterizing joint effects of spatial extent, temperature magnitude and duration of heat waves and cold spells over Central Europe, Int. J. Climatol., 35, 1232–1244, https://doi.org/10.1002/joc.4050, 2015.

Lhotka, O., Kyselý, J., and Plavcová, E.: Evaluation of major heat waves' mechanisms in EURO-CORDEX RCMs over Central Europe, Clim. Dyn., 50, 4249–4262, https://doi.org/10.1007/s00382-017-3873-9, 2018.

Liang, X., Xie, Z., and Huang, M.: A new parameterization for surface and groundwater interactions and its impact on water budgets with the variable infiltration capacity (VIC) land surface model, Journal of Geophysical Research: Atmospheres, 108, https://doi.org/https://doi.org/10.1029/2002JD003090, 2003.

Liu, X., He, B., Guo, L., Huang, L., and Chen, D.: Similarities and Differences in the Mechanisms Causing the European Summer Heatwaves in 2003, 2010, and 2018, Earth's Future, 8, e2019EF001386, https://doi.org/10.1029/2019EF001386, 2020.

Lorenz, R., Stalhandske, Z., and Fischer, E. M.: Detection of a Climate Change Signal in Extreme Heat, Heat Stress, and Cold in Europe From Observations, Geophys. Res. Lett., 46, 8363–8374, https://doi.org/10.1029/2019GL082062, 2019.

Manabe, S. and Delworth, T.: The temporal variability of soil wetness and its impact on climate, Climatic Change, 16, 185–192, https://doi.org/10.1007/BF00134656, 1990.

Martínez-de la Torre, A. and Miguez-Macho, G.: Groundwater influence on soil moisture memory and land–atmosphere fluxes in the Iberian Peninsula, Hydrol. Earth Syst. Sci., 23, 4909–4932, https://doi.org/10.5194/hess-23-4909-2019, 2019.

Masson-Delmotte, V., Zhai, P., Pirani, A., Connors, S., Péan, C., Berger, S., Caud, N.and Chen, Y., Goldfarb, L., Gomis, M., Huang, M., Leitzell, K., Lonnoy, I., Matthews, J., Maycock, T., Waterfield, T., Yelekçi, O., Yu, R., and B., Z., eds.: IPCC report, Climate Change 2021: The Physical Science Basis. Contribution of Working Group I to the Sixth Assessment Report of the Intergovernmental Panel on Climate Change, Cambridge University Press, Cambridge, United Kingdom and New York, NY, USA, https://www.ipcc.ch/report/ar6/wg1/downloads/report/IPCC_AR6_WGI_FullReport.pdf, 2021.

Mauritsen, T., Bader, J., Becker, T., and et al.: Developments in the MPI-M Earth System Model version 1.2 (MPI-ESM1.2) and Its Response to Increasing CO2, J. Adv. Model. Earth Syst., 11, 998–1038, https://doi.org/10.1029/2018MS001400, 2019.

Maxwell, R. M.: A terrain-following grid transform and preconditioner for parallel, large-scale, integrated hydrologic modeling, Adv. Water. Resour., 53, 109–117, https://doi.org/10.1016/j.advwatres.2012.10.001, 2013.

Maxwell, R. M. and Condon, L. E.: Connections between groundwater flow and transpiration partitioning, Science, 353, 377–380, https://doi.org/10.1126/science.aaf7891, 2016.

Maxwell, R. M. and Miller, N. L.: Development of a Coupled Land Surface and Groundwater Model, J. Hydrometeorol., 6, 233–247, https://doi.org/10.1175/JHM422.1, 2005.

Maxwell, R. M., Chow, F. K., and Kollet, S. J.: The groundwater–land-surface–atmosphere connection: Soil moisture effects on the atmospheric boundary layer in fully-coupled simulations, Advances in Water Resources, 30, 2447–2466, https://doi.org/10.1016/j.advwatres.2007.05.018, 2007.

Mearns, L. O., Lettenmaier, D. P., and McGinnis, S.: Uses of Results of Regional Climate Model Experiments for Impacts and Adaptation Studies: the Example of NARCCAP, Curr. Clim. Change Rep., 1, 1–9, https://doi.org/10.1007/s40641-015-0004-8, 2015.

Miralles, D. G., van den Berg, M. J., Teuling, A. J., and de Jeu, R. A. M.: Soil moisture-temperature coupling: A multiscale observational analysis, Geophys. Res. Lett., 39, L21707, https://doi.org/10.1029/2012GL053703, 2012.

Molina, M. O., Sánchez, E., and Gutiérrez, C.: Future heat waves over the Mediterranean from an Euro-CORDEX regional climate model ensemble, Sci. Rep., 10, 8801, https://doi.org/10.1038/s41598-020-65663-0, 2020.

Mu, M., De Kauwe, M. G., Ukkola, A. M., Pitman, A. J., Guo, W., Hobeichi, S., and Briggs, P. R.: Exploring how groundwater buffers the influence of heatwaves on vegetation function during multi-year droughts, Earth Syst. Dyn., 12, 919–938, https://doi.org/10.5194/esd-12-919-2021, 2021.

Mu, M., Pitman, A. J., De Kauwe, M. G., Ukkola, A. M., and Ge, J.: How do groundwater dynamics influence heatwaves in southeast Australia?, Weather and Climate Extremes, 37, 100 479, https://doi.org/10.1016/j.wace.2022.100479, 2022.

Myhre, G., Alterskjær, K., Stjern, C. W., Hodnebrog, Ø., Marelle, L., Samset, B. H., Sillmann, J., Schaller, N., Fischer, E., Schulz, M., and Stohl, A.: Frequency of extreme precipitation increases extensively with event rareness under global warming, Sci. Rep., 9, 16063, https://doi.org/10.1038/s41598-019-52277-4, 2019.

Nairn, J. R. and Fawcett, R. J. B.: The excess heat factor: a metric for heatwave intensity and its use in classifying heatwave severity, Int. J. Environ. Res. Public Health, 12, 227–253, https://doi.org/10.3390/ijerph120100227, 2014.

Naumann, G., Cammalleri, C., Mentaschi, L., and Feyen, L.: Increased economic drought impacts in Europe with anthropogenic warming, Nat Clim Chang, 11, 485–491, https://doi.org/10.1038/s41558-021-01044-3, 2021.

Niu, G.-Y., Yang, Z.-L., Dickinson, R. E., Gulden, L. E., and Su, H.: Development of a simple groundwater model for use in climate models and evaluation with Gravity Recovery and Climate Experiment data, J. Geophys. Res. Atmos., 112, D07103, https://doi.org/10.1029/2006JD007522, 2007.

Oleson, K., Dai, Y., Bonan, G. B., Bosilovichm, M., Dickinson, R., Dirmeyer, P., and et al.: Technical Description of the Community Land Model (CLM) (No. NCAR/TN-461+STR), Tech. rep., University Corporation for Atmospheric Research, https://doi.org/10.5065/D6N877R0, 2004.

Oleson, K. W., Niu, G.-Y., Yang, Z.-L., Lawrence, D. M., Thornton, P. E., Lawrence, P. J., Stöckli, R., Dickinson, R. E., Bonan, G. B., Levis, S., Dai, A., and Qian, T.: Improvements to the Community Land Model and their impact on the hydrological cycle, J. Geophys. Res. Biogeosci., 113, G01021, https://doi.org/10.1029/2007JG000563, 2008.

Pal, J. S. and Eltahir, E. A. B.: Pathways Relating Soil Moisture Conditions to Future Summer Rainfall within a Model of the Land–Atmosphere System, Journal of Climate, 14, 1227 – 1242, https://doi.org/https://doi.org/10.1175/1520-0442(2001)014<1227:PRSMCT>2.0.CO;2, 2001.

Perkins, S. E. and Alexander, L. V.: On the Measurement of Heat Waves, J. Clim., 26, 4500–4517, https://doi.org/10.1175/JCLI-D-12-00383.1, 2013.

Perkins, S. E., Alexander, L. V., and Nairn, J. R.: Increasing frequency, intensity and duration of observed global heatwaves and warm spells, Geophys. Res. Lett., 39, L20714, https://doi.org/10.1029/2012GL053361, 2012.

Perkins-Kirkpatrick, S. E. and Lewis, S. C.: Increasing trends in regional heatwaves, Nat. Commun., 11, 3357, https://doi.org/10.1038/s41467-020-16970-7, 2020.

Plavcová, E. and Kyselý, J.: Overly persistent circulation in climate models contributes to overestimated frequency and duration of heat waves and cold spells, Clim. Dyn., 46, 2805–2820, https://doi.org/10.1007/s00382-015-2733-8, 2016.

Pothapakula, P. K., Primo, C., Sørland, S., and Ahrens, B.: The synergistic impact of ENSO and IOD on Indian summer monsoon rainfall in observations and climate simulations – an information theory perspective, Earth Syst. Dynam., 11, 903–923, https://doi.org/10.5194/esd-11-903-2020, 2020.

Prein, A. F., Gobiet, A., Truhetz, H., Keuler, K., Goergen, K., Teichmann, C., Fox Maule, C., van Meijgaard, E., Déqué, M., Nikulin, G., Vautard, R., Colette, A., Kjellström, E., and Jacob, D.: Precipitation in the EURO-CORDEX 0.11° and 0.44° simulations: high resolution, high benefits?, Clim. Dyn., 46, 383–412, https://doi.org/10.1007/s00382-015-2589-y, 2016.

Rockel, B., Will, A., and Hense, A.: The Regional Climate Model COSMO-CLM (CCLM), Meteorol. Z., 17, 347–348, https://doi.org/10.1127/0941-2948/2008/0309, 2008.

Rummukainen, M.: Added value in regional climate modeling, WIREs Clim. Change, 7, 145–159, https://doi.org/10.1002/wcc.378, 2016.

Russo, S., Sillmann, J., and Fischer, E. M.: Top ten European heatwaves since 1950 and their occurrence in the coming decades, Environ. Res. Lett., 10, 124003, https://doi.org/10.1088/1748-9326/10/12/124003, 2015.

Schlemmer, L., Schär, C., Lüthi, D., and Strebel, L.: A Groundwater and Runoff Formulation for Weather and Climate Models, J. Adv. Model. Earth Syst., 10, 1809–1832, https://doi.org/10.1029/2017MS001260, 2018.

Schulz, J.-P., Vogel, G., Becker, C., Kothe, S., Rummel, U., and Ahrens, B.: Evaluation of the ground heat flux simulated by a multi-layer land surface scheme using high-quality observations at grass land and bare soil, Meteorol. Z., 25, 607–620, https://doi.org/10.1127/metz/2016/0537, 2016.

Seneviratne, S. I., Lüthi, D., Litschi, M., and Schär, C.: Land–atmosphere coupling and climate change in Europe, Nature, 443, 205–209, https://doi.org/10.1038/nature05095, 2006.

Seneviratne, S. I., Corti, T., Davin, E. L., Hirschi, M., Jaeger, E. B., Lehner, I., Orlowsky, B., and Teuling, A. J.: Investigating soil moisture–climate interactions in a changing climate: A review, Earth-Science Reviews, 99, 125–161, https://doi.org/10.1016/j.earscirev.2010.02.004, 2010.

Shrestha, P., Sulis, M., Masbou, M., Kollet, S., and Simmer, C.: A Scale-Consistent Terrestrial Systems Modeling Platform Based on COSMO, CLM, and ParFlow, Mon. Weather Rev., 142, 3466–3483, https://doi.org/10.1175/MWR-D-14-00029.1, 2014.

Song, Y. M., Wang, Z. F., Qi, L. L., and Huang, A. N.: Soil Moisture Memory and Its Effect on the Surface Water and Heat Fluxes on Seasonal and Interannual Time Scales, J. Geophys. Res. Atmos., 124, 10 730–10 741, https://doi.org/10.1029/2019JD030893, 2019.

Sørland, S. L., Schär, C., Lüthi, D., and Kjellström, E.: Bias patterns and climate change signals in GCM-RCM model chains, Environ. Res. Lett., 13, 074017, https://doi.org/10.1088/1748-9326/aacc77, 2018.

Stegehuis, A. I., Vogel, M. M., Vautard, R., Ciais, P., Teuling, A. J., and Seneviratne, S. I.: Early Summer Soil Moisture Contribution to Western European Summer Warming, J. Geophys. Res. Atmos., 126, e2021JD034646, https://doi.org/10.1029/2021JD034646, 2021.

Steger, C. and Bucchignani, E.: Regional Climate Modelling with COSMO-CLM: History and Perspectives, Atmosphere, 11, 1250, https://doi.org/10.3390/atmos11111250, 2020.

Stott, P. A., Stone, D. A., and Allen, M. R.: Human contribution to the European heatwave of 2003, Nature, 432, 610–614, https://doi.org/10.1038/nature03089, 2004.

Strathearn, M., Osborne, N. J., and Selvey, L. A.: Impact of low-intensity heat events on mortality and morbidity in regions with hot, humid summers: a scoping literature review, Int. J. Biometeorol., 66, 1013–1029, https://doi.org/10.1007/s00484-022-02243-z, 2022.

Sulikowska, A. and Wypych, A.: Summer temperature extremes in Europe: how does the definition affect the results?, Theor. Appl. Climatol., 141, 19–30, https://doi.org/10.1007/s00704-020-03166-8, 2020.

Taylor, K. E., Stouffer, R. J., and Meehl, G. A.: An Overview of CMIP5 and the Experiment Design, Bull. Am. Meteorol. Soc., 93, 485–498, https://doi.org/10.1175/BAMS-D-11-00094.1, 2012.

Teuling, A. J., Uijlenhoet, R., van den Hurk, B., and Seneviratne, S. I.: Parameter Sensitivity in LSMs: An Analysis Using Stochastic Soil Moisture Models and ELDAS Soil Parameters, Journal of Hydrometeorology, 10, 751–765, https://doi.org/10.1175/2008JHM1033.1, 2009.

Tomczyk, A. M. and Bednorz, E.: Heat waves in Central Europe and their circulation conditions, Int. J. Climatol., 36, 770–782, https://doi.org/10.1002/joc.4381, 2016.

Torma, C., Giorgi, F., and Coppola, E.: Added value of regional climate modeling over areas characterized by complex terrain—Precipitation over the Alps, Journal of Geophysical Research: Atmospheres, 120, 3957–3972, https://doi.org/https://doi.org/10.1002/2014JD022781, 2015.

Valcke, S.: The OASIS3 coupler: a European climate modelling community software, Geosci. Model Dev., 6, 373–388, https://doi.org/10.5194/gmd-6-373-2013, 2013.

van der Linden, P. and Mitchell, J. F. B.: ENSEMBLES: Climate Change and Its Impacts – Summary of Research and Results from the ENSEMBLES Project, Met Office Hadley Centre, FitzRoy Road, Exeter EX1 3PB, UK, http://ensembles-eu.metoffice.com/docs/Ensembles_final_report_Nov09.pdf, 2009.

Vautard, R., Yiou, P., D'Andrea, F., de Noblet, N., Viovy, N., Cassou, C., Polcher, J., Ciais, P., Kageyama, M., and Fan, Y.: Summertime European heat and drought waves induced by wintertime Mediterranean rainfall deficit, Geophys. Res. Lett., 34, L07711, https://doi.org/10.1029/2006GL028001, 2007.

Vautard, R., Gobiet, A., Jacob, D., and et al.: The simulation of European heat waves from an ensemble of regional climate models within the EURO-CORDEX project, Clim. Dyn., 41, 2555–2575, https://doi.org/10.1007/s00382-013-1714-z, 2013a.

Vautard, R., Noël, T., Li, L., Vrac, M., Martin, E., Dandin, P., Cattiaux, J., and Joussaume, S.: Climate variability and trends in downscaled high-resolution simulations and projections over Metropolitan France, Clim. Dyn., 41, 1419–1437, https://doi.org/10.1007/s00382-012-1621-8, 2013b.

Vogel, M. M., Zscheischler, J., and Seneviratne, S. I.: Varying soil moisture–atmosphere feedbacks explain divergent temperature extremes and precipitation projections in central Europe, Earth System Dynamics, 9, 1107–1125, https://doi.org/10.5194/esd-9-1107-2018, 2018.

Vogt, J., Soille, P., De Jager, A., Rimaviciute, E., Mehl, W., Foisneau, S., Bodis, K., Dusart, J., Paracchini, M., Haastrup, P., and Bamps, C.: A pan-European River and Catchment Database, JRC Reference Report, Joint Research Centre, Institute for Environment and Sustainability, https://doi.org/10.2788/35907, 2007.

Voldoire, A., Sanchez-Gomez, E., Salas y Mélia, D., and et al: The CNRM-CM5.1 global climate model: description and basic evaluation, Clim. Dyn., 40, 2091–2121, https://doi.org/10.1007/s00382-011-1259-y, 2013.

Yang, L., Sun, G., Zhi, L., and Zhao, J.: Negative soil moisture-precipitation feedback in dry and wet regions, Sci Rep, 8, 4026, https://doi.org/10.1038/s41598-018-22394-7, 2018.

Yeh, P. J.-F. and Eltahir, E. A. B.: Representation of Water Table Dynamics in a Land Surface Scheme. Part I: Model Development, Journal of Climate, 18, 1861–1880, https://doi.org/10.1175/JCLI3330.1, 2005.

Yin, C., Yang, Y., Chen, X., Yue, X., Liu, Y., and Xin, Y.: Changes in global heat waves and its socioeconomic exposure in a warmer future, Clim. Risk Manag., 38, 100 459, https://doi.org/10.1016/j.crm.2022.100459, 2022.

Yule, E. L., Hegerl, G., Schurer, A., and Hawkins, E.: Using early extremes to place the 2022 UK heat waves into historical context, Atmos. Sci. Lett., p. e1159, https://doi.org/10.1002/asl.1159, 2023.

Zhang, R., Sun, C., Zhu, J., Zhang, R., and Li, W.: Increased European heat waves in recent decades in response to shrinking Arctic sea ice and Eurasian snow cover, NPJ Clim. Atmos. Sci., 3, 7, https://doi.org/10.1038/s41612-020-0110-8, 2020.

Zhang, X., Hegerl, G., Zwiers, F., and Kenyon, J.: Avoiding Inhomogeneity in Percentile-Based Indices of Temperature Extremes, J. Clim., 38, 1641–1651, https://doi.org/10.1175/JCLI3366.1, 2005.

Zhang, X., Alexander, L., Hegerl, G. C., Jones, P., Tank, A. K., Peterson, T. C., Trewin, B., and Zwiers, F. W.: Indices for monitoring changes in extremes based on daily temperature and precipitation data, WIREs Clim. Change, 2, 851–870, https://doi.org/10.1002/wcc.147, 2011.